Deep-Sea Research I 75 (2013) 93–109

Contents lists available at SciVerse ScienceDirect

Deep-Sea Research I

journal homepage: www.elsevier.com/locate/dsri

Megafaunal distribution and assessment of total methane and sulfide consumption by mussel beds at Menez Gwen hydrothermal vent, based on geo-referenced photomosaics

Y. Marcon [a,*], H. Sahling [a], C. Borowski [b], C. dos Santos Ferreira [a], J. Thal [a], G. Bohrmann [a]

[a] MARUM—Center for Marine Environmental Sciences and Faculty of Geosciences, University of Bremen, Klagenfurter Straße, D-28359 Bremen, Germany
[b] Max Planck Institute for Marine Microbiology, Celsiusstr. 1, D-28359 Bremen, Germany

ARTICLE INFO

Article history:
Received 18 July 2012
Received in revised form
21 January 2013
Accepted 28 January 2013
Available online 4 February 2013

Keywords:
Photomosaic
Bathymodiolus azoricus
Menez Gwen
Hydrothermal vent
Biomass
Chemical consumption
Fluid flow

ABSTRACT

The Menez Gwen hydrothermal vents, located on the flanks of a small young volcanic structure in the axial valley of the Menez Gwen seamount, are the shallowest known vent systems on the Mid-Atlantic Ridge that host chemosynthetic communities. Although visited several times by research cruises, very few images have been published of the active sites, and their spatial dimensions and morphologies remain difficult to comprehend. We visited the vents on the eastern flank of the small Menez Gwen volcano during cruises with RV Poseidon (POS402, 2010) and RV Meteor (M82/3, 2010), and used new bathymetry and imagery data to provide first detailed information on the extents, surface morphologies, spatial patterns of the hydrothermal discharge and the distribution of dominant megafauna of five active sites. The investigated sites were mostly covered by soft sediments and abundant white precipitates, and bordered by basaltic pillows. The hydrothermally-influenced areas of the sites ranged from 59 to 200 m^2. Geo-referenced photomosaics and video data revealed that the symbiotic mussel *Bathymodiolus azoricus* was the dominant species and present at all sites. Using literature data on average body sizes and biomasses of Menez Gwen *B. azoricus*, we estimated that the *B. azoricus* populations inhabiting the eastern flank sites of the small volcano range between 28,640 and 50,120 individuals with a total biomass of 50 to 380 kg wet weight. Based on modeled rates of chemical consumption by the symbionts, the annual methane and sulfide consumption by *B. azoricus* could reach 1760 mol CH_4 yr^{-1} and 11,060 mol H_2S yr^{-1}. We propose that the chemical consumption by *B. azoricus* over at the Menez Gwen sites is low compared to the natural release of methane and sulfide via venting fluids.

1. Introduction

Hydrothermal vents were first discovered in 1977 and have been the focus of many studies since then (Lutz and Kennish, 1993; Van Dover, 2000). Especially the discovery of non-photosynthesis-fueled ecosystems associated with these systems, with abundant and diverse endemic fauna, excited the interest of a multitude of scientists from various disciplines. However, hydrothermal vent systems are located in depths without natural sunlight where the field of view for researchers and cameras diving with submersibles or remotely operated vehicles (ROV) is extremely limited despite the use of powerful lights. Hence, more than 30 years after the first discovery, the overall structure of hydrothermal venting sites and the distribution of the associated fauna are often only known from images providing close-up views of limited sections of vents, while only very few detailed maps of entire sites have been published (Barreyre et al., 2012; Bell et al., 2012; Escartín et al., 2008).

Detailed descriptions of the distribution of the faunal assemblages at hydrothermal vent systems that are available in the literature are mostly based on drawings or geo-referenced GIS layers that are drawn from video data. Such data are available in particular from the Endeavor hydrothermal field on the Juan de Fuca Ridge (Juniper et al., 1998; Sarrazin et al., 1997), from the Broken Spur vent field (Copley et al., 1997) and the Logatchev site on the Mid-Atlantic Ridge (MAR) (Gebruk et al., 2000a), and from the Lucky Strike system, at which the faunal distribution on a large chimney structure was described (Cuvelier et al., 2009). Such maps give valuable qualitative information on the distribution of the faunal patches and the layout of the sites but they rely on hand drawings from observations of video material and precision of inferred areas of cover is likely to be limited. Some works (Durand et al., 2002; Juniper et al., 1998; Sarrazin et al., 1997), however, focused particularly on the issue of improving

* Correspondence to: Universität Bremen, GEO Gebäude, Raum 1130, Klagenfurter Straße, 28359 Bremen, Germany. Tel.: +49 421 218 65055; fax: +49 421 218 65099.
E-mail addresses: ymarcon@marum.de, yann.marcon@gmail.com (Y. Marcon).

0967-0637/$ - see front matter © 2013 Elsevier Ltd. All rights reserved.
http://dx.doi.org/10.1016/j.dsr.2013.01.008

the accuracy of spatial measurements from video imaging by drawing the contours on a background geology map of the site. In those cases, geo-referencing data of the basemap were obtained either from passive reference markers that were captured on video images (Durand et al., 2002) or from long baseline (LBL) navigation data that were correlated to the images (Delaney et al., 1992; Sarrazin and Juniper, 1998; Sarrazin et al., 1997). All these methods can be very efficient and can be applied in areas with sharp topographic contrasts.

An alternative approach is to use geo-referenced photo-mosaics to map the faunal distribution. Image mosaicking involves assembling several overlapping images together to form a composite image of a larger scene. The mosaic is then geo-referenced into a geographic information system (GIS), and areas can be computed. Such a method can provide a significantly quicker way to study areas with low to moderate relief. In addition, contours of features of interest can be drawn onto the geo-referenced image material directly. Similar methods have been used to successfully map faunal communities at different scales and in various types of environments. Examples include large-scale studies of faunal distribution at the Håkon Mosby Mud Volcano (Jerosch et al., 2007, 2006) and at the Regab pockmark (Olu-Le Roy et al., 2007), and small-scale studies at the Chowder Hill mound on the Juan de Fuca Ridge (Grehan and Juniper, 1996), at cold seeps in the Gulf of Mexico (Lessard-Pilon et al., 2010a, 2010b) and at discrete sites of hydrothermal activity on the Eastern Lau Spreading Center (Podowski et al., 2009).

Analyses of hydrothermal fauna usually focus on the distribution of the assemblages or on population structure in relation to the environment, and sometimes give density and biomass estimates per unit areas (Lutz and Kennish, 1993; Ramirez Llodra et al., 2007). However, the overall spatial distributions of faunal assemblages and animal abundances or biomasses at entire vent sites have rarely been quantified (e.g. Gebruk et al., 2000a; Podowski et al., 2009). Such knowledge is valuable as it gives information on the size of hydrothermal faunal populations, and can be used to infer chemical consumption rates. In a context where seabed methane emissions are considered to contribute noticeably to the global carbon budget (Judd, 2003), it is important to evaluate the relative significance of faunal methane consumption against methane effluxes in hot fluid emissions.

In this study, we use high-resolution bathymetry data together with areal photomosaics to provide for the first time detailed maps and descriptions of five sites of active venting from the Menez Gwen system in the area of the previously reported marker position PP30/31 (Desbruyères et al., 2001). The Menez Gwen hydrothermal vent field was chosen for this study because it is a volcanic structure where hydrothermal activity was believed to be concentrated over small areas. It has been visited by several cruises and the faunal communities hosted by the vent field have been the focus of many biological studies (Comtet and Desbruyères, 1998; Dixon et al., 2001; Fouquet et al., 1994; Riou et al., 2010; Sarradin et al., 2001, 1999; Shank and Martin, 2003; Von Cosel et al., 1999). However, descriptions and images of the sites of venting activity remain poor and quantitative data on dimensions, size of populations and biomasses are scarce.

Ship- and autonomous underwater vehicle- (AUV) based bathymetry surveys were conducted in September–October 2010 during cruises POS402 and M82/3 to the Menez Gwen hydrothermal vent field on the Mid-Atlantic Ridge. Five sites of active venting activity were intensively studied during twenty ROV dives. Using GIS, we provide measurements of surfaces covered by dominant species of megafauna, and estimates of the minimum biomass of *Bathymodiolus azoricus*. Also, we use published values of size, density and substrate uptake rates for *B. azoricus* at Menez Gwen to infer total methane and sulfide consumption rates at the scale of a vent site. The final goal of this study is to assess the significance of faunal methane and sulfide consumption against natural methane and sulfide release within vent fluids.

2. Site description

The Menez Gwen segment of the Mid-Atlantic Ridge is about 55 km long (Parson et al., 2000), and stretches from 38°03′N to 37°35′N in a S-SW to N-NE direction (Fig. 1). A large volcano with a mean diameter of 15 km is present near the center of the segment, and it reaches up to about 800 m above the surrounding seafloor (Fig. 1a). The top part is divided into two halves by a 9-km long axial graben of similar orientation to the ridge segment that forms a 300 to 400-m deep and 2-km wide valley across the volcano.

Several recently formed minor volcanoes are scattered across the northern part of the graben. The largest of them is about 1 km wide, up to 200 m high (Fig. 1b) and its highest point reaches up to 800 m water depth. The surface rocks of this young volcano are composed of fresh lava and some volcanic breccia (Fouquet et al., 1995; Ondréas et al., 1997). The lava has no sediment cover and it has been suggested that the entire small volcano built up during the latest eruptive episode (Ondréas et al., 1997). The hydrothermal activity at Menez Gwen is mainly concentrated on the southern and eastern flanks of this small volcano (Fig. 1b) (Charlou et al., 2000; Desbruyères et al., 2001). Although the Menez Gwen hydrothermal vents have been visited several times by research cruises, information on the morphology and geological composition of active sites is scarce and concentrates on two locations on the southern flank of the volcano (Fig. 1b). One of them (PP10/F11) is characterized by a 50-m wide mound with a low elevation and 2-m high anhydrite chimneys, which are surrounded by barite-rich precipitates; the other (D9, PP11, F12) is an escarpment topped by a chimney, which is bordered by pillow lava and crumbled rock (Charlou et al., 2000; Desbruyères et al., 2001; Fouquet et al., 1997, 1994). Such information is not available for sites on the eastern volcano flank.

Menez Gwen is part of the Azores Marine Park and possible future access restrictions to the southern sites may lead future research to focus on the eastern area. The sites of hydrothermal activity studied during the cruise M82/3 (2010) were therefore located in this area. More specifically, they were located on the eastern flank of the small volcano close to its summit (Fig. 1b and c), and between 850 and 814 m depth. In 20 dives, five major sites were found in the area: Atos 10, Cage Site, Marker 4, White Flames, and Woody. Apart from Atos 10, which was named after a marker deployed during the ATOS cruise in 2001 (Sarradin et al., 2001), the site names were those assigned during the cruise M82/3 in September–October 2010.

Large megafauna is composed of the bivalve species *Bathymodiolus azoricus*, the caridean shrimps *Chorocaris chacei*, *Mirocaris fortunata* and *Alvinocaris* sp. aff. *stactophila*, numerous gastropods, mainly *Lepetodrilus atlanticus* and *Protolira valvatoides*, the crab *Segonzacia mesatlantica* and the large non-hydrothermal crab *Chaceon affinis* (Desbruyères et al., 2001; Galkin and Goroslavskaya, 2010; Gebruk et al., 2000b; Ramirez Llodra et al., 2000; Von Cosel et al., 1999). Smaller animals are even more diverse (Galkin and Goroslavskaya, 2010), but are not discernible in video and photo materials.

3. Methods

3.1. Bathymetric surveys

Swath-mapping surveys were conducted during the M82/3 cruise with the hull-mounted multi-beam echosounder (MBES)

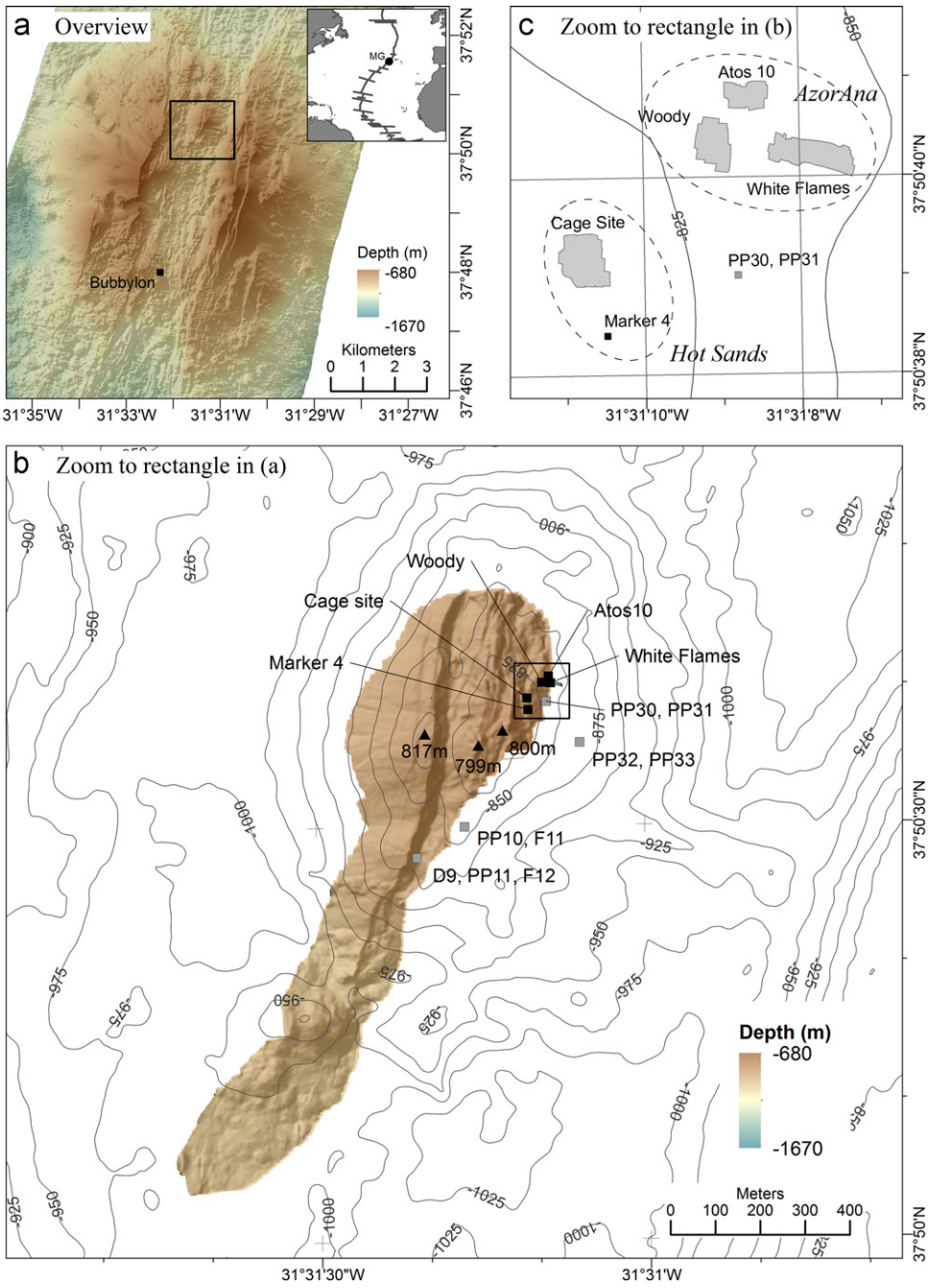

Fig. 1. (a) Overview map of the Menez Gwen volcano showing the ship-borne bathymetry (10 m grid size) acquired during the M82/3 cruise (2010); the insert shows the location of the Menez Gwen volcano on the Mid-Atlantic Ridge, and the rectangle indicates the location of the area shown in (b); the Bubbylon site was discovered during the M82/3 cruise; (b) AUV-based micro-bathymetry (2.5 m grid size) of the young volcano (highest elevations are highlighted with black triangles) and individual sites of active venting studied during the M82/3 cruise (black squares); the sites described by Desbruyères et al. (2001) are also plotted (gray squares); according to published data, the D9, PP11, F12 sites, and possibly the PP10, F11 sites, are also known as 'Fontaine', 'Mogued Gwen', 'Menez Flank' and 'Montmartre' (Charlou et al., 2000); however, these sites lie well to the south of our study area; the rectangle indicates the location of the area shown in (c); (c) outline and relative position of the photomosaics.

EM122 from Kongsberg Maritime operating at 12 kHz with 432 beams. Micro-bathymetry was acquired during the POS402 cruise with the MARUM AUV SEAL 5000, using a RESON SeaBat 7125 multibeam echosounder operating at 400 kHz with 512 beams. Processing of the bathymetry data was done with MB-System (Caress and Chayes, 2001).

3.2. Imagery, mosaicking and image processing

Imagery used for the production of mosaics was acquired with a DSPL SSC 6500 Colorzoom video camera with corrected optics to eliminate geometric and chromatic distortions. The DSPL camera was mounted on a pan-and-tilt head at the front of the ROV Quest 4000 m (MARUM). For mosaicking applications, the camera was positioned as vertically as possible without having parts of the ROV within the view. In this position, the angle of the optical axis of the camera in relation to the vertical plane was 39 degrees; therefore every image was affected by the same perspective distortion. Laser pointers were used throughout the surveys to ensure that scale information was recorded with the imagery.

Images were obtained along parallel and overlapping transects at a constant speed and a steady altitude across each site. Photomosaics

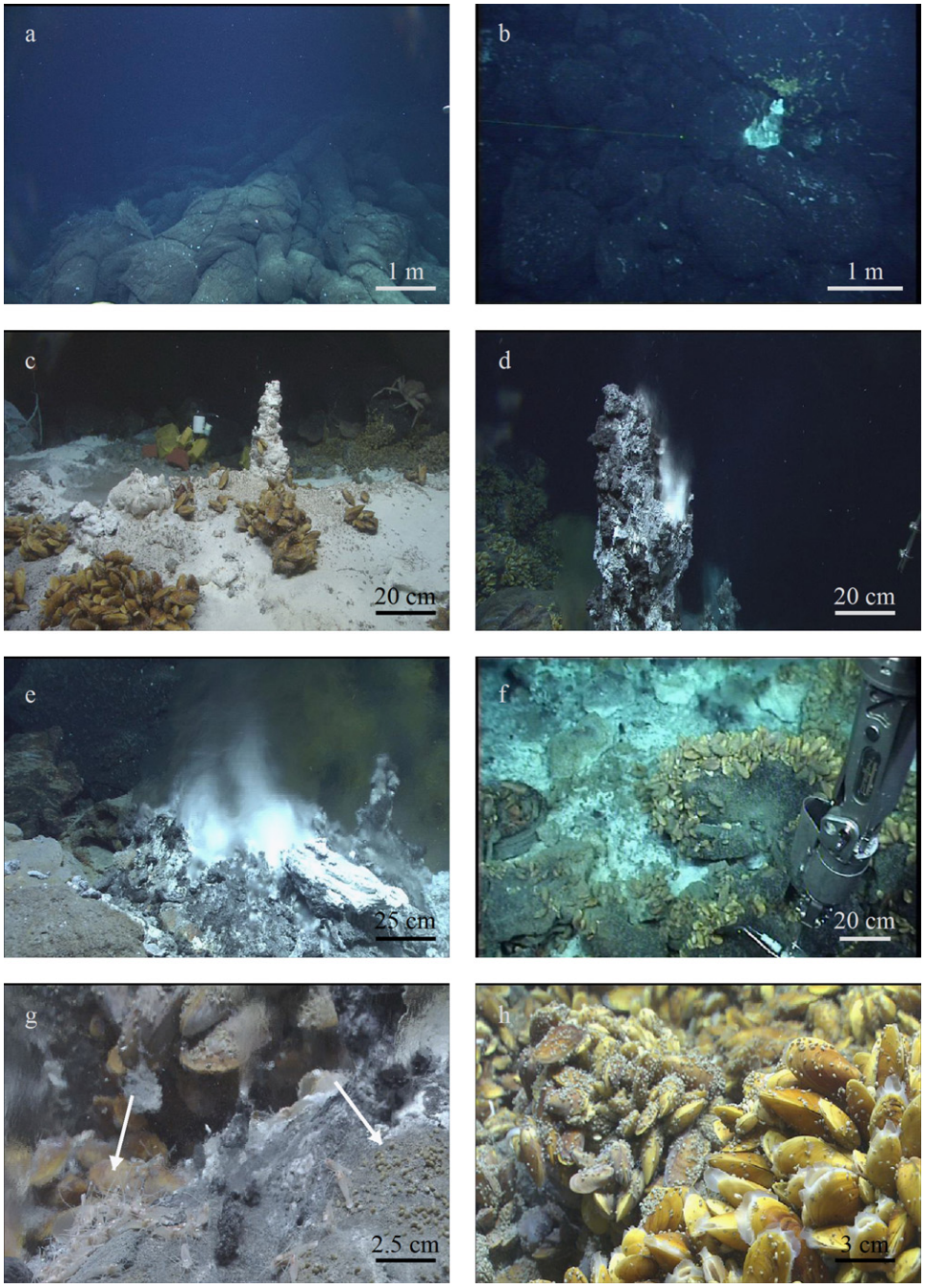

Fig. 2. Seafloor images taken by ROV Quest (courtesy Marum). For all images scale bars apply to the foreground. (a) Pillow lava (dive 281); (b) unnamed mini-site of venting activity halfway between Woody and White Flames (dive 286); (c) center of the main mound at Woody covered with anhydrite precipitates; the chimney structure showed no active venting; the greyish speckle around the bottom of the chimney is caused by a high abundance of gastropods (dive 293); (d, e) chimney structure and hydrothermal fluid close to boiling point at the top of White Flames (dive 276); (f) basaltic rock covered with mussels on the side facing the hot fluid chimney, and bare on the opposite side (dive 295); (g) swarm of shrimps and gastropods on rocks around hot fluid emissions (dive 289); (h) *Bathymodiolus azoricus* with high (background) and low (foreground) gastropods abundance on their shells (dive 281).

were constructed using consecutive frames from the video files, with an overlap of 25–30%. Individual transects of the mosaics were constructed using a MATLAB algorithm (Pizarro and Singh, 2003) provided by C. Fisher and E. Podowski. This algorithm was developed to cope with the peculiarities of the underwater environment (low lighting, adverse motion of the camera such as roll, pitch and yaw) and is relatively well suited to compensate for inaccuracies between consecutive images that would be related to the camera inclination. The final mosaics were constructed manually with Photoshop by assembling individual transects together. Drift-induced errors between transects were low (about 50 cm error every 10 m in flat areas, i.e. 5%) due to the small dimensions of the mosaics. Nevertheless, where possible, registration artifacts were positioned away from the main areas of interest in order to ensure the best possible matches in the most active areas of the study sites. For each mosaic, colors and contrasts were enhanced using ImageJ software (Abramoff et al., 2004).

3.3. GIS and spatial analyses

Mosaics were geo-referenced in ArcGIS using navigation data of the ROV Quest. Ultra-short baseline (USBL) data were used for

Table 1
Ranges of values for all parameters concerning *Bathymodiolus azoricus* at Menez Gwen, which are used in this study; minimum and maximum calculated values are based respectively on the lowest and highest limits of assumed shell length and population density; refer to text of detailed explanations.

Parameter	Range	Type	Source
Shell length (mm)	40–80	Assumption	Comtet and Desbruyères (1998)
Population density (ind m^{-2})	400–700	Assumption	Colaço et al. (1998)
Weight (g wet wt ind^{-1})	1.78–7.56	Calculated	From Martins et al. (2008)
Biomass (kg wet wt m^{-2})	0.71–5.3	Calculated	From Martins et al. (2008)
Gill weight (g dry wt ind^{-1})	0.09–0.36	Calculated	From Martins et al. (2008)
CH_4 uptake (μmol d^{-1} ind^{-1})	5.9–96.1	Calculated	From Martins et al. (2008)
H_2S uptake (μmol d^{-1} ind^{-1})	36.5–604.1	Calculated	From Martins et al. (2008)

the relative positioning of each site, whereas dead-reckoning navigation data from the Doppler Velocity Log (DVL) sensor were used for scaling and orientating the mosaics. Information from laser pointers was used to confirm correct scaling of the mosaics.

For all mosaics, interpreted features were delineated and polygons were created in ArcGIS to map the spatial distribution of each feature. Mapped features include hard and soft substrata, patches of mussels or shells, and zones of intense whitish mineral precipitation. Total areas of each site were measured in ArcGIS and correspond to the limit of the hydrothermal deposits and fauna. The extent of mussel communities was delineated, areas and percentages of cover were calculated. All areas were measured using a Mollweide equal area projection.

Additional qualitative observations made from all high-resolution video and photo material from cruise M82/3 were pinpointed onto the mosaics. Point features that were mapped include locations of the exit points of fluid emission, and qualitative assessments of abundance of some mobile fauna. Points of fluid emission were sorted depending on the presence or absence of chimney structure and, where relevant, on the height of the chimneys. Additionally, wherever the videos showed the seafloor close enough to reliably observe the presence or absence of shrimps and gastropods, the observation was marked in the mosaics. Animal abundances were assessed semi-quantitatively. Shrimp abundance was categorized according to absence, low abundance (1–10 ind m^{-2}) and high abundance (>10 ind m^{-2}). Gastropods were present at all sites and therefore divided into two categories of low abundance (individuals are scattered, substrate is clearly visible between individuals) and high abundance (gastropods build closed groups, substrate not visible between individuals). This work was performed for all five sites but the amounts of observation points at Atos 10 and Marker 4 were too low (<5) for interpretation; therefore the results are not shown. However, data from every site were used for the analyses of abundance against distance to points of fluid emission. The resolution of the mosaic images did not allow an identification of shrimps and gastropods to species level. Therefore, our analyses only used the informal categories 'shrimp' and 'gastropods'.

3.4. Estimations of *B. azoricus* biomass, methane and sulfide consumption

Total population and total biomass of *B. azoricus* were estimated for all sites (except Marker 4), based on our measured values of mussel coverage and on estimated mussel sizes and densities. From our observations, mussel patches included various sizes from juveniles to largest individuals of ca. 12 cm shell length. We did not analyze representative values for population densities and size frequencies of the mussels; however, our collections revealed that small juveniles and very large individuals were rare, while the majority of the animals were medium sized. This corresponded to published data based on collections in several years and at different seasons. According to these data the shell lengths for the majority of individuals at Menez Gwen ranged between 40 and 80 mm (Comtet and Desbruyères, 1998). Population density in *B. azoricus* mussel patches at Menez Gwen has been estimated 400 to 700 ind m^{-2} (Colaço et al., 1998). Based on these estimates of *B. azoricus* shell size and population density, biomass estimations range between 0.71 and 5.3 kg wet wt m^{-2} (Martins et al., 2008).

We used these values (Table 1) to estimate population sizes and total biomasses of *B. azoricus* for each site, except for Marker 4, for which the perspective distortion of the mosaic did not allow calculating areas. The population size estimates were based on the extents of mussel coverage measured on 2D images from the various sites. As these images do not account for the bottom relief, the calculated population sizes are possibly underestimated. Furthermore, as biomass estimates were additionally based on a range representative of the most frequent shell sizes and not on real size frequency distributions, the total areal biomasses are also very likely underestimated and represent minimum values.

Our calculations of methane and sulfide consumption by the mussels are based on published values of chemical uptake rates by *B. azoricus* at Menez Gwen. We followed the modeling results of Martins et al. (2008) and used uptake rates of 5.9 to 96.1 μmol CH_4 d^{-1} ind^{-1} and 36.5 to 604.1 μmol H_2S d^{-1} ind^{-1} (Table 1). These values were modeled based on estimated average volatile concentrations in Menez Gwen mussel habitats of 100 μM methane and 60 μM sulfide (Martins et al., 2008; Sarradin et al., 1998), and on maximum uptake rates of methane and sulfide of 742 and 4596.5 μmol g^{-1} gill dry wt d^{-1} (I. Martins personal comm.). According to Martins et al. (2008), maximum uptakes rates could only be reached by the largest mussel specimens (≥ 110 mm SL), and with CH_4 and H_2S concentrations about three times higher than those estimated within the Menez Gwen habitats. Therefore, in order to constrain our estimates, we chose ranges of uptake values that are representative of the majority of the mussel population, and do not consider under-represented extreme values (low and high).

3.5. Estimations of focused fluid flow rates

Focused fluid flow rates at Menez were estimated from the mosaics, the dive videos, and published estimates of fluid velocities (Sarrazin et al., 2009). Indeed, the imagery data gave a reasonable overview of the number and distribution of discrete fluid outflows at each site. At some of them, mainly with chimney structures, hot fluid vigorously discharged in the form of a distinct plume clearly visible on the images. However, in most cases we could neither visualize the contours nor estimate the basal diameters of the plumes of venting fluids. Moreover, observations showed that the height of the chimneys could not be used as a proxy for plume size. Therefore we were not able to assess the relative strength of focused discharges between sites. Nevertheless, based on our observations of high definition dive videos,

we estimated 24 plume diameters (out of 92 discrete outflows), which ranged from about 0.5 cm up to 12 cm (median=2 cm, mean=2.2 cm, SD=2.5 cm). Assuming that discrete outflows are circular, corresponding areas range from 0.2 cm^2 to 113.1 cm^2 (median=3.1 cm^2, mean=8.6 cm^2, SD=22.5 cm^2).

Unfortunately fluid flow velocity measurements do not exist for the Menez Gwen system. Published fluid velocity measurements in other hydrothermal systems give broad ranges of values: velocities range from 100 to 6200 mm/s in discrete sources and from 1.1 to 150 mm/s in diffuse sources (Sarrazin et al., 2009). Therefore, focused fluid sources are likely to yield outflows of between 62 $m^3\,yr^{-1}$ and $2.2\times10^6\,m^3\,yr^{-1}$. However, these boundary estimations are based on extreme diameter values that are not representative of the typical plume size at Menez Gwen, which according to the median value is close to 2 cm (area=3.1 cm^2). The median is less influenced by extreme values than the mean, and hence is more representative of the most common type of focused source. Indeed, using the mean area value (8.6 cm^2) in our calculations would lead to a great overestimation of the global fluid flow, since the large majority of discrete outflows are around 3.1 cm^2 in area. Therefore, for our estimation of minimum fluid flow at the scale of the studied sites, we chose to use the median value of plume diameter (2 cm) and the low range limit velocity of 100 mm/s. In this case, an average focused source at Menez Gwen is likely to yield a minimum outflow of 991 $m^3\,yr^{-1}$.

The values chosen for plume diameters and fluid velocities are aimed at providing a low range estimation of global focused fluid flow rates. Furthermore, considering that some discrete fluid outflows may not have been spotted, final fluid flow estimates are likely to be underestimated.

4. Results

4.1. Visual and geophysical site descriptions

The high-resolution bathymetry data gathered during cruises POS402 and M82/3 in 2010 showed that the inner volcano is bisected by a fracture in a SW-NE direction similar to that of the graben (Fig. 1a and b). According to visual exploration, several additional N-NE striking fractures cross the eastern summit of the volcano, with few steep, meter-high slopes covered with broken pillow tubes. The dive videos also disclosed an inner volcano mostly covered by sediment-free pillow lavas (Fig. 2a) likely resulting from recent volcanic events, while the grabens mainly are filled with talus material. These fractures suggest apparently that the topography in this area was shaped by a combination of volcanic and tectonic events. Furthermore, such fractures are likely to provide preferential pathways for the hydrothermal fluids. Some parts of the eastern side of the young volcano, and particularly in the close vicinity of the sites of hydrothermal activity, are dominated by talus of broken pillows and areas of breccia. In general, the pillows were not or only sparsely covered by sediment, except at the sites of active venting, which were covered by sandy material.

The five sites investigated in the study are grouped spatially into two clusters (Fig. 1c). The first cluster comprises Woody, Atos 10,

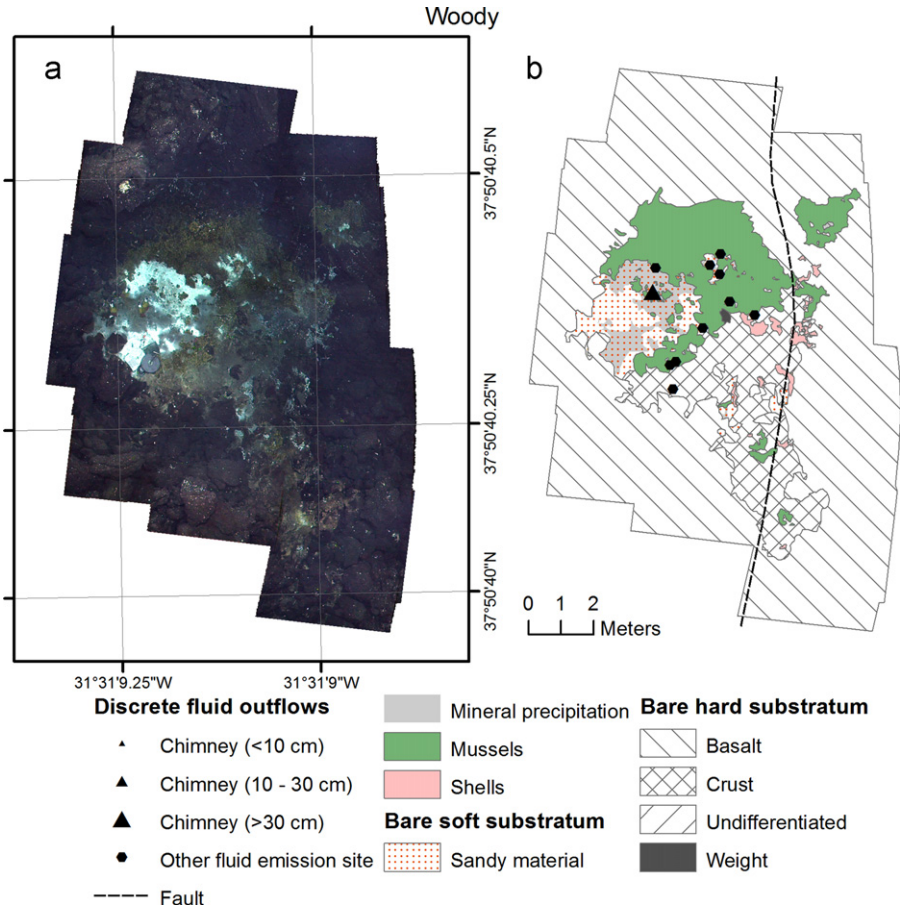

Fig. 3. Representations of the Woody hydrothermal vent site: (a) photomosaic, (b) schematic. The main chimney represented on the schematic was inactive at the time of the cruise M82/3. 'Other fluid emission site' refers to sites where localized emission of hot fluid was observed, but without a chimney structure. This site is characterized by a break-in-slope in the topography, likely related to a fault.

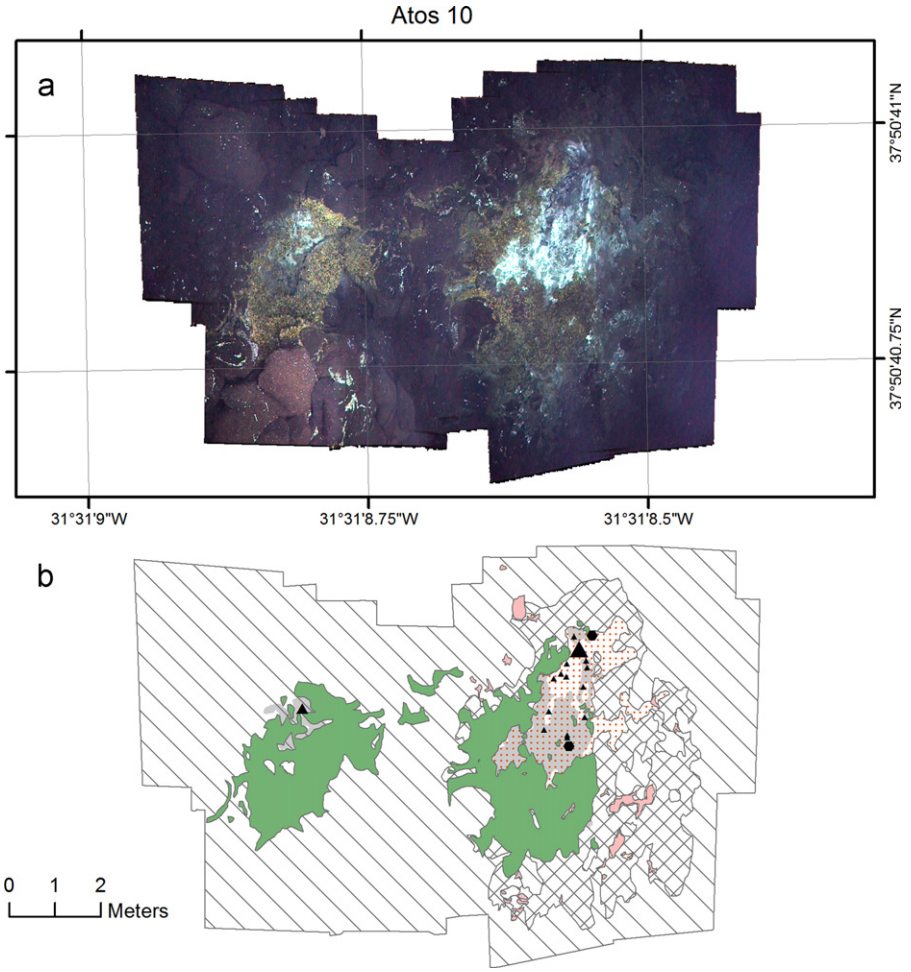

Fig. 4. Representations of the Atos 10 hydrothermal vent site: (a) photomosaic, (b) schematic; for detailed explanations, see legend of Fig. 3. Atos 10 is composed of two sites; the eastern site is characterized by a mound of sandy material, covered with abundant white precipitates and with focused outflows. The western site is devoid of soft sediments and developed around a single chimney; Mussels are abundant at both sites.

and White Flames (Figs. 3–5). This cluster also includes some minor sites of active venting, in particular between White Flames and Woody (Fig. 2b). The alignment of some of these sites suggests that hydrothermal activity in this area is structurally controlled. The second cluster, which includes the sites Marker 4 and Cage Site, is located about 50 m to the southwest and closer to the summit of the volcano (Figs. 6 and 7). Mosaics were constructed for all five sites, and the full resolution GeoTIFF files of the corresponding geo-referenced mosaics are provided as electronic supplements.

4.1.1. *Woody (37°50′40.4″N, 31°31′9.4″W)*

The Woody site (Fig. 3) is about 829 m deep and has a total area of 69 m^2 (Table 2). The site is composed of a main mound structure and two small areas of minor venting activity. The topography in this zone is dipping gently toward east to a break in slope and then flattening on the east of the site. The main mound is located in the slope and is characterized by an almost flat circular center dipping strongly down to the break in slope on its east side. The break in slope could be the result of a normal fault running across the site in a north-south direction, and it is likely related to one of the larger fractures that cross the volcano. Based on the videos, the vertical displacement was estimated to less than two meters. Such a fault may provide preferred pathways for the hydrothermal fluids.

The main mound appeared devoid of boulders, and was covered by a sandy material and slabs and crusts. Its center was about 4.5 m in diameter and white precipitates covered large parts of it. The main chimney was about 50 cm high and was located on the center part. In contrast to the chimneys of the other study sites, the chimney at Woody did not seem recently active (Fig. 2c). It was entirely white, likely due to anhydrite precipitates, and no vent fluid was observed coming out of the chimney during the cruise M82/3. The most active sites of fluid exit were observed around the chimney, from small fractures and from within the mussel patches. Bivalves were present in thick layers and they were mostly restricted to hard surfaces. Nevertheless, they did not cover every rock surface that surrounded the main mound; pillows on the western and southwestern sides were entirely bare, and rocky surfaces on the northeastern side supported most of the bivalve population (Fig. 3a). In terms of surface, almost 25% of the total area was covered by mussels (Table 2). The maximum distance between the mussel beds and the hot fluid exits did not exceed 2.5 m. According to our estimations, the mussel population and total biomass at Woody range from 6800 to 11,900 ind and from 12.1 to 90 kg wet wt, respectively (Table 3). The smaller active emission sites were located at 6 and 8 m from the center of the main mound. Both were very close to the break in slope and slightly to the east of it. They were characterized by a very small center covered with white precipitates surrounded by mussels *B. azoricus*. A sandy covering was not visible.

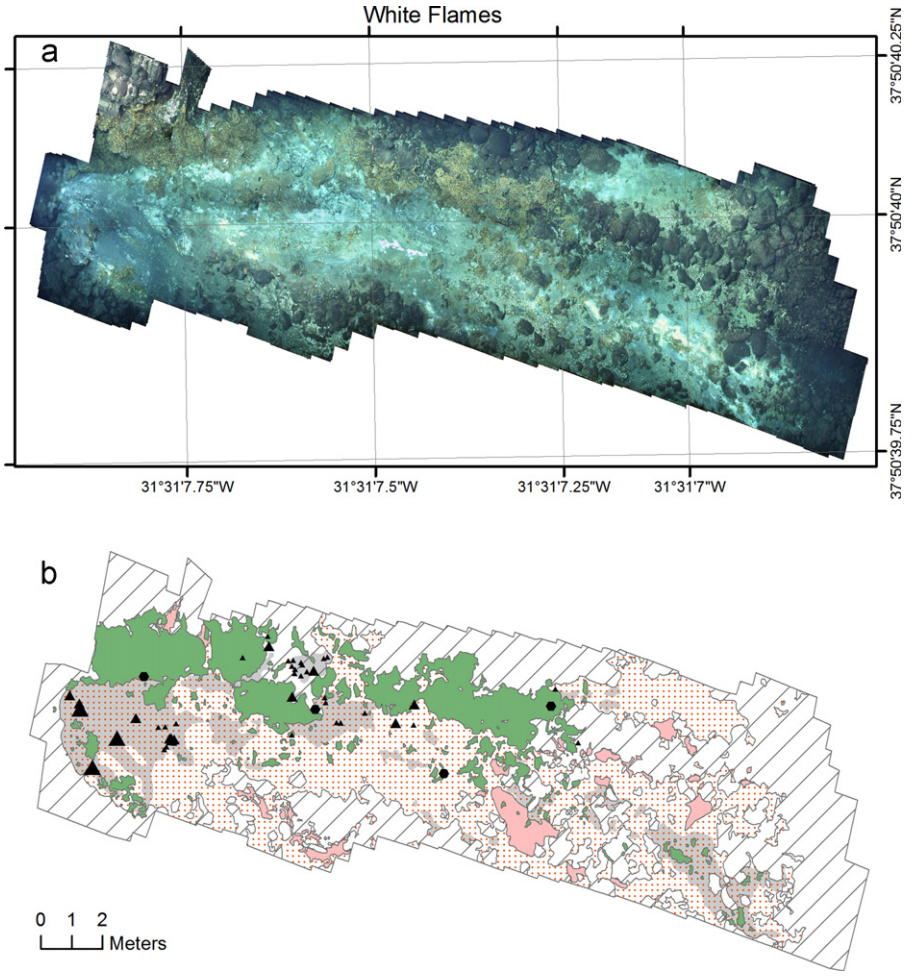

Fig. 5. Representations of the White Flames hydrothermal vent site: (a) photomosaic, (b) schematic; for detailed explanations, see legend of Fig. 3. The White Flames site developed along a steep slope and is topped by high chimneys; sandy material and white mineral precipitates are abundant; mussels are mostly distributed on basaltic boulders along the northern side of the site.

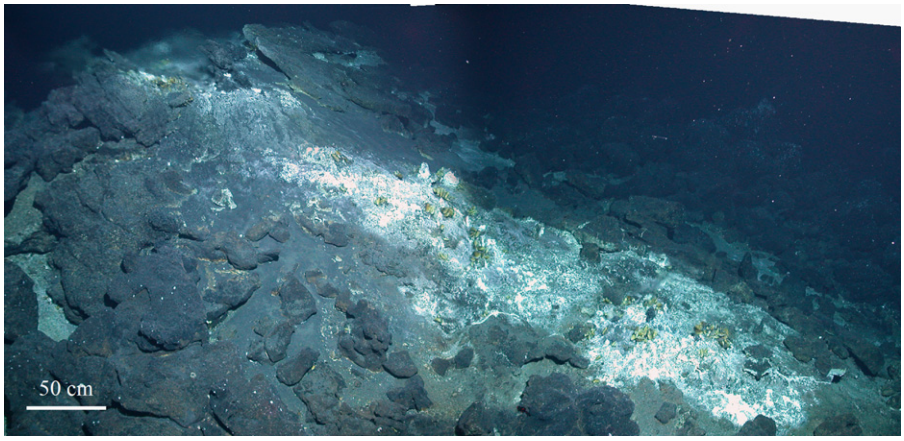

Fig. 6. Photomosaic of Marker 4; active venting occurs at the top of the site (indicated by blurry water). Downslope from there white precipitates form a 4 m-long and 1 m-wide stripe. Mussels are present in small aggregations (<20 ind) mostly located on the white precipitates.

4.1.2. Atos 10 (37°50′40.8″N, 31°31′8.8″W)

Atos 10 is located at a depth of 828 m, covers an area of 59 m^2 (Table 2), and is composed of a major eastern site and a minor western site, about 5 m apart (Fig. 4a). Experiments and colonization cages had been deployed at Atos 10 during the French/Portuguese/British Atos cruise in 2001 and earlier French/Portuguese research cruises (Dixon et al., 2001; Sarradin et al., 2001). The site was clearly identified by the presence of old mooring weights.

The major eastern site formed a circular mound of about 4 m in diameter, slightly elevated compared to the surrounding ground, and devoid of large pillows. The central part was largely covered by white precipitates and scattered with 13 chimneys, most of them very small (less than 5 cm). One chimney on the

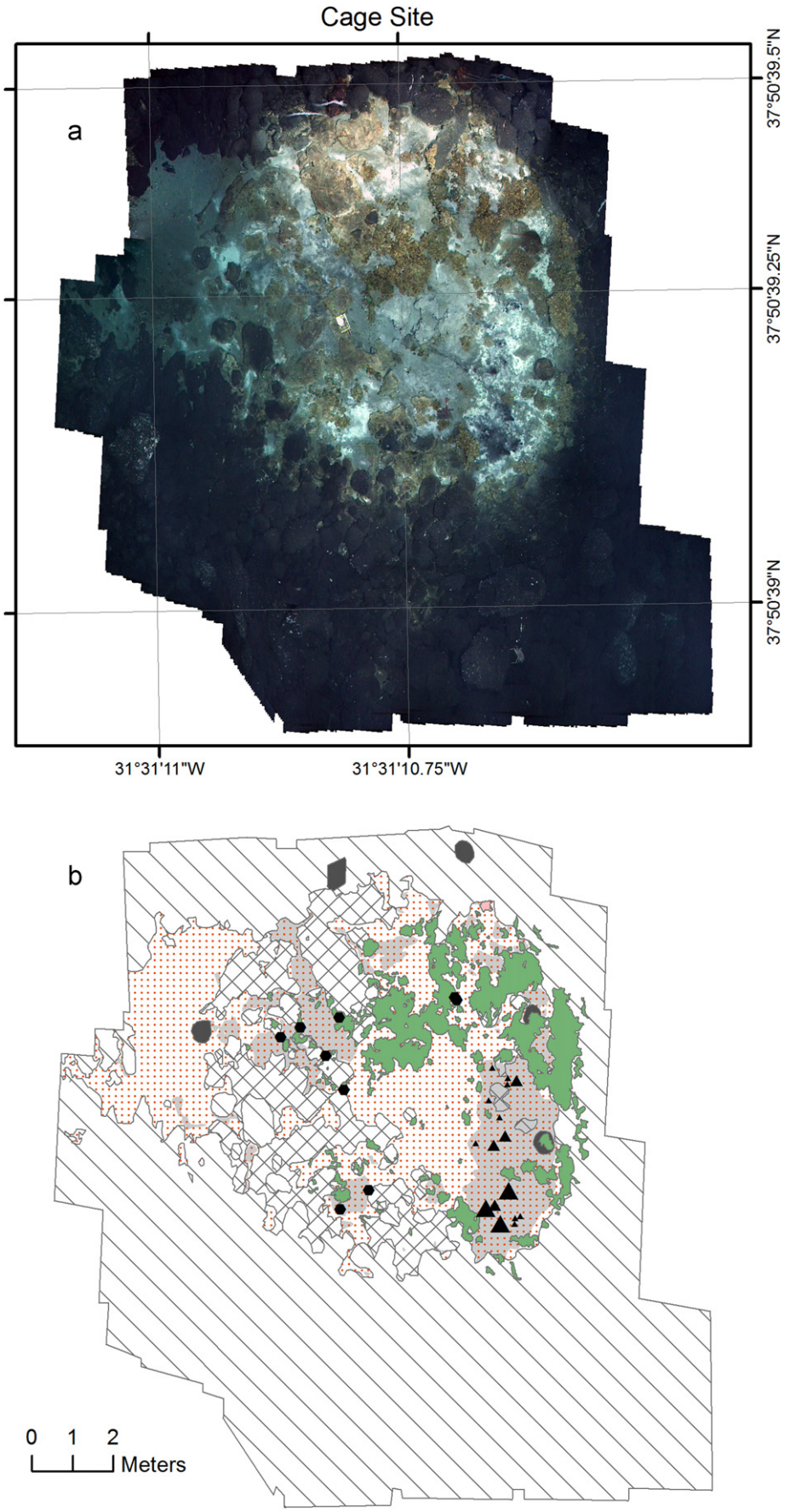

Fig. 7. Representations of the Cage Site hydrothermal vent site: (a) photomosaic, (b) schematic; for detailed explanations, see legend of Fig. 3. Cage site is a single W-NW dipping oval mound covered by sandy material and slabs of barite-rich crusts. The site is characterized by the presence of a depression (4 m^2) near its center. East of the depression is the most active area, as indicated by the presence of chimneys and abundant white precipitates.

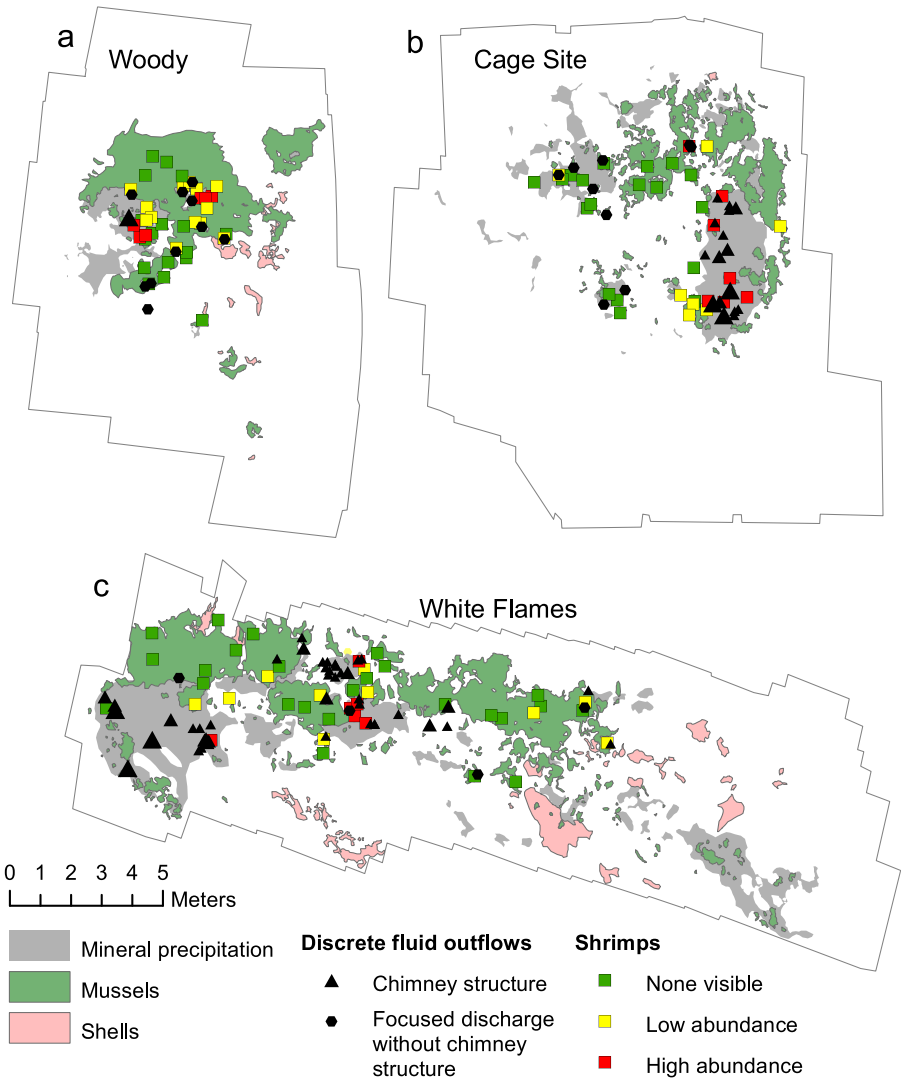

Fig. 8. Shrimp distribution at (a) Woody, (b) Cage Site and (c) White Flames. The shrimp distribution pattern is similar at all sites, and shows a strong correlation with the presence of focused fluid outflows; high shrimp abundance occurs within 1 m of hot fluid outflows.

Table 2
Characteristics of the sites and mussel covers.

Site	Approx. depth (m)	Area (m^2)	Discrete sources with chimneys	Discrete sources without chimneys	Mussel cover (m^2)	Mussel cover (%)
Woody	829	69	1 (inactive?)	7	17	24.6
Atos 10	828	59	13	2	13.2	22.4
White Flames	835–850	199	43	4	29.1	14.6
Cage Site	813.5	100	16	7	12.3	12.3
Marker 4	812	20–30	?	?	–	–

northern edge of the mound was significantly larger, reaching up to about 50 cm in height. *Bathymodiolus azoricus* covered the rim of the main mound, and the abundance of this species increased with the distance to the chimneys and to the main area of hot fluid emission. The largest and thickest cover of bivalves was observed in the south and southwestern edges of the mound (Fig. 4b). In total, this bivalve covered 22.4% of the total area of the Atos 10 site (Table 2). The western site involved only fluid emission and did not form a mound. It consisted of a single 15–20 cm high chimney, which had grown between basaltic pillows. Sandy or crusty material was absent. White precipitates were visible on the pillows in the close vicinity of the chimney, over an area of about 0.5 m^2. Surrounding rocks were densely covered by *B. azoricus* over an area of about 6 m^2. Bivalve aggregations at Atos 10 were never observed farther than 3.2 m from the hot fluid exits. According to our estimations, mussel population and total biomass at Atos 10 range from 5280 to 9240 ind and from 9.4 to 69.9 kg wet wt respectively (Table 3).

4.1.3. *White Flames (37°50′40.3″N, 31°31′8.6″W)*

White Flames (Fig. 5) is located about 20 m to the west of Woody and is the largest of the Menez Gwen sites investigated during the M82/3 cruise, with an area of 199 m^2 (Table 2). This site was

characterized by several chimneys of various sizes (5 cm to 1 m high) expelling hot fluids and gas bubbles that are considered to represent the gaseous phase separated by subsurface boiling. These emissions brightly reflected ROV lights and gave the impression of burning flares (Fig. 2d and e). The site extended over 25 m in a west to east direction, and had an approximate width of 6 m. The elevation decreased regularly from west to east with a relatively strong gradient. The difference in altitude was estimated from the navigation data of the ROV to be 15 m, which corresponded to a mean slope gradient of 60% between the western/top and eastern/bottom ends of the site.

The highest chimney (about 0.8–1 m high) was located at a depth of 835 m and marked the western and top end of White Flames. More chimneys were observed downslope towards east. Their numbers and sizes decreased in a downslope direction. The site was mostly covered by sands and gravels with a few pillows of basalt. Barite-rich crusts were also visible. White mineral precipitates indicating diffuse fluid flow were present in many places around the chimneys and towards the bottom of the site (Fig. 5a and b).

Bivalves covered 14.6% of the White Flames area and this coverage was low compared to the other sites in the same cluster. (Table 2, Fig. 5b). The bivalve distribution did not extend to all zones where diffuse fluid discharge was expected to occur, and seemed limited to hard substrates, such as basaltic pillows and crusts that were in the upper two-thirds of the slope. In this area, the northern side of the site was bordered by large basaltic structures that grew larger and higher nearer the top of the site, thus creating jagged vertical surfaces that overlooked the main areas of hot fluid emission. Those structures were heavily covered by bivalves and, based on the mosaics, represented more than 90% of the total bivalve cover at White Flames. The main aggregations of mussels were constantly observed within 2.8 m from a hot fluid exit. According to our estimations, mussel population and total biomass at White Flames range from 11,640 to 20,370 ind and from 20.7 to 154.1 kg wet wt respectively (Table 3).

4.1.4. Marker 4 (37°50′38.4″N, 31°31′10.7″W)

Marker 4, located in 812 m water depth, is the smallest of the five investigated sites (Table 2). The mosaics of Marker 4 were composed of images from the forward-looking cameras. They were strongly impacted by perspective distortion and GIS georeferencing was therefore not possible (Fig. 6). The size of the site was assessed at 20–30 m^2 from navigation data. Hot fluid was emitted from small chimneys at the top of the site. From that point, a stripe of white hydrothermal deposits extended over about 4 m down-slope towards the east. The slopes were partly covered by sandy deposits, and slabs of crusts were visible that stuck out around the top of the site. Iron oxides could be seen over the surrounding rocks. Marker 4 harbored only a few mussels scattered individually or in patches of less than 20 animals over the white deposits. Their abundance was negligible compared to the other sites.

4.1.5. Cage Site (37°50′39.2″N, 31°31′10.7″W)

Cage Site (Fig. 7a) is located at 813.5 m water depth and covers 100 m^2 (Table 2). It was used for mooring deployments during earlier cruises, and was easily identified from remaining ground weights. This site consisted mainly of a single W-NW dipping oval mound (9–9.5 m diam.) that was protruding slightly from the surrounding basaltic pillows. A few basaltic pillows were scattered on the higher part, in the southeastern corner of the mound, while the rest was covered by sandy material and slabs of barite-rich crust. Located south-east of the mound center was a large (4 m^2) depression, less than 1 m deep and covered by soft sediments. On the western side the sediment cover extended up to 2 m away from the edge of the mound (Fig. 7b). White precipitates related to fluid flow were unevenly distributed on the mound surface. The most intense venting occurred on the highest part of the site. In this area, hot fluid was emitted from several chimneys, which were all located within an 8-m^2 large

Table 3
Minimum and maximum estimated mussel population, total biomass, and annual consumptions of methane and sulfide by *Bathymodiolus azoricus*; minimum estimates are based on the lowest limits of shell length (SL=40 mm) and density (400 ind m^{-2}), whereas maximum estimates rely on the highest limits (SL=80 mm, density=700 ind m^{-2}).

Site	Population size (ind)	Total biomass (kg wet wt)	CH_4 uptake by *B. azoricus* (mol yr^{-1})	H_2S uptake by *B. azoricus* (mol yr^{-1})
Woody	6800–11,900	12.1–90	15–418	91–2626
Atos 10	5280–9240	9.4–69.9	11–324	70–2039
White Flames	11,640–20,370	20.7–154.1	25–715	155–4494
Cage Site	4920–8610	8.7–65.1	11–302	66–1890
Total	28,640–50,120	50.9–379.1	62–1759	382–11,059

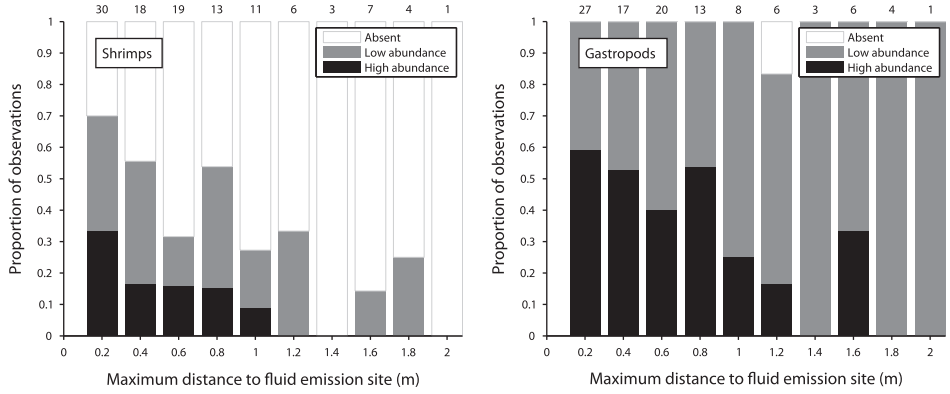

Fig. 9. Variation of the abundance of shrimps (left) and gastropods (right) with the distance to the closest hot fluid exit; the values above the bars represent on the left plot the total amount of observations of abundance.

area of high mineral precipitation. In other areas of high mineral precipitation, hot fluid emission was only observed from fractures or from under slabs of barite (Fig. 7b). *Bathymodiolus azoricus* were concentrated within 2.8 m of hot fluid exits and covered about 12% of the site area (Table 2). Mussels settled predominantly on rock surfaces that were orientated towards the fluid emissions while the central depression was almost bare of bivalves (Fig. 2f). Mussel patch sizes ranged from dense aggregations of hundreds of *B. azoricus* to single individuals. According to our estimations, mussel population and total biomass at Cage Site range from 4920 to 8610 ind and from 8.7 to 65.1 kg wet wt respectively (Table 3).

4.2. Occurrences of other fauna visible on video materials

Shrimps usually occurred at all sites around fluid emission and occasionally also in mussel beds. High shrimp densities (>10 ind m^{-2}) were always related to hot fluid discharge and occurred within a radius of 1 m around the fluid source during all observations (Figs. 8 and 9). Animals were concentrated in dense swarms in close proximity to single hot fluid emissions (Fig. 2g) or spread more evenly over larger areas with several smaller point sources. These swarms were located next to hot fluid emissions at all sites (Figs. 8 and 9) and were particularly common near some chimneys of White Flames. However, shrimp were not present at each hot discharge locations; for instance, shrimps were not observed close to the larger chimneys at the top of White Flames. At Cage Site and Woody, the shrimp spread over larger areas where hot fluids were emitted from several small sources.

Gastropods were observed at all sites on mussel shells and hard rock surfaces (Fig. 2h). While close-up photos revealed that they were also present on soft substrates, they were not reliably discernible on the mosaic images because the contrast resolution was not sufficient. Gastropods were patchily distributed. Dense aggregations were observed on rocks and mussel shells next to hot fluid emissions and along the path of the hot fluid flows (Fig. 9 and 10). Only a few centimeters to decimeters away, the density of gastropods dropped sharply. Videos showed that gastropods were constantly moving and that their distribution pattern was thereby very dynamic.

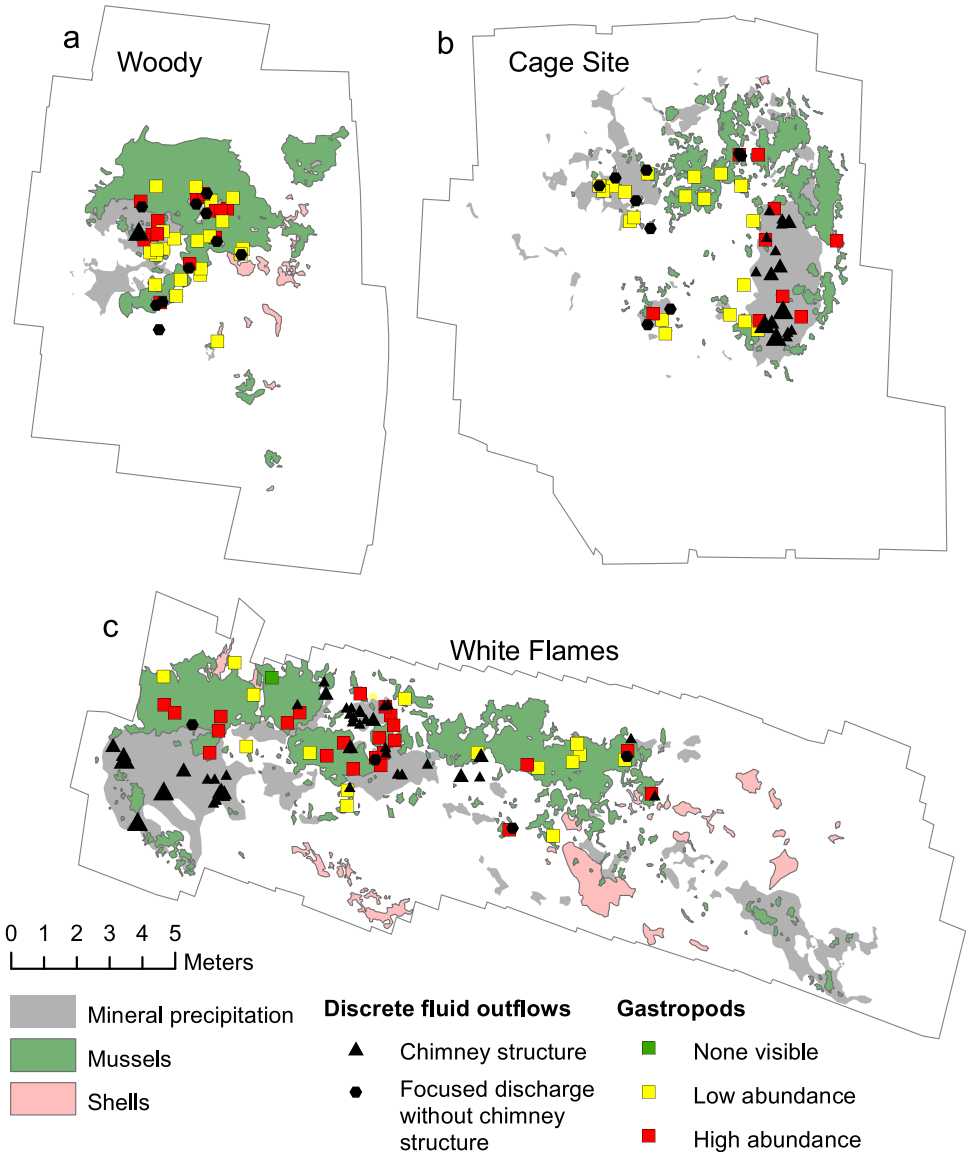

Fig. 10. Gastropod abundance at (a) Woody, (b) Cage Site and (c) White Flames. The gastropod distribution pattern is similar at all sites, and is related to the presence of fluid flow; dive videos showed that the gastropod abundance drops sharply a few centimeters only away from the distance to hot fluid (see text).

5. Discussion

5.1. Mosaics for site identification

Hydrothermal activity at Menez Gwen has been described at two areas on the southern and eastern flanks of the inner volcano (Charlou et al., 2000; Desbruyères et al., 2001). The sites studied in this work correspond to the active vent area on the eastern flank that is referred to as marker PP30/31 in the literature (Desbruyères et al., 2001; Riou et al., 2010), but we were not able to unequivocally relocate this site. Therefore our investigation sites may not be identical to the originally described marker positions, but it is also possible that the original markers were not anymore in place. Clear identification of bottom weights at Atos 10 and Cage Site that had been left from cage moorings deposited during the ATOS cruise in 2001 indicated that these sites were identical to locations of earlier work (Dixon et al., 2001; Sarradin et al., 2001). The sites named by Charlou et al. (2000) lie well to the south of our study area (Fig. 1). In total, five sites were found on the eastern flank, and a mosaic was built for each of them. The area was intensively investigated during twenty dives and it is unlikely that other major sites were missed in the close vicinity.

We used USBL navigation, which is known to suffer from temporary inaccuracies of up to tens of meters offset from the real positions. However, occasional outliers in our navigation data were leveled for a total of 20 dives at the investigation sites to guarantee reliable navigation data. The mosaics presented here provide an additional basis for future identification of the vent sites on the eastern flank of the young Menez Gwen volcano, and this information will compensate for possible inaccuracies of underwater navigation.

A loss of quality is commonly introduced during the mosaicking process. Indeed, where adjacent frames overlap, images are seamlessly blended together (Pizarro and Singh, 2003). However, small registration errors may occur, which can cause some fuzziness in parts of the mosaics. The schematics of the sites (Figs. 3b, 4b, 5b, 7b) compensate for this loss of quality by showing the most important features of each site.

5.2. Faunal distribution

Mussels preferentially settled on rock surfaces and rarely on hydrothermal deposits. This is in accordance with previous observations around the marker sites PP10/F11 on the southern volcano flank and PP32/33 on the eastern flank (Desbruyères et al., 2001). The mussels predominantly concentrated on rock surfaces exposed to the vent fluid flow. This was particularly obvious at Cage Site where only rock surfaces facing fluid emanations were densely covered by mussels while other surfaces of the same rocks were entirely bare of mussels (Figs. 2f and 7b). The distribution of the bivalves was therefore highly controlled by site morphologies and exposure of rock surfaces to fluid flow. However, *B. azoricus* avoided close contact with focused vent fluids and were scarcely present in the immediate vicinity of the focused fluid discharge. Maximum distances between mussel aggregations and hot fluid exits ranged between 2.5 and 3.2 m. This matched earlier observations at the Eiffel Tower edifice in Lucky Strike where *B. azoricus* always kept a distance of at least 25 cm from hot fluid exits, and where mussel beds and clumps were never observed farther than about 3 m from black smokers (Cuvelier et al., 2009).

Conversely, shrimps occurred mostly within the hot fluid and in the very close vicinity of the emission sites. High abundances of shrimps were never observed farther than in 1 m distance from a fluid exit point. This is comparable to earlier observations at Lucky Strike. There, swarms of shrimps occurred within 1.25 m distance to black smokers and 50 cm distance to flanges and diffusion zones (Cuvelier et al., 2009).

Shrimp species could not be identified from the images. However, *Chorocaris chacei*, *Mirocaris fortunata*, and *Alvinocaris* sp. aff. *stactophila* have been found in Menez Gwen before (Colaço et al., 1998; Gebruk et al., 2000b). All of them have different feeding behaviors (Gebruk et al., 2000b; Ramirez Llodra et al., 2000) and this certainly controls their distribution. *C. chacei* and *M. fortunata* have been observed previously on chimney walls at Lucky Strike (Cuvelier et al., 2009; Gebruk et al., 2000b) and it is very likely that both species existed also among the shrimps we detected next to hot fluid discharge. *C. chacei* scavenges and also carries episymbiotic micro-organisms, which are considered chemoautotrophic and most likely add to the nutrition of their hosts (Gebruk et al., 2000b; Ramirez Llodra et al., 2000). Therefore, it is reasonable that *C. chacei* aggregated next to hot fluids in Menez Gwen where the chemosynthetic bacteria should have good access to diluted sulfide. *M. fortunata* grazes on bacteria on sulfide surfaces and also feeds on detritus and fecal deposits of *Bathymodiolus* (Gebruk et al., 2000b; Ramirez Llodra et al., 2000). Accordingly, this species may have been present among the dense shrimp aggregates around hot fluid discharge sites and also among the scattered shrimp individuals in the mussel beds. The feeding habits of *A.* sp. aff. *stactophila* are unknown, but *Alvinocaris* species in general are predators and opportunistic feeders and they are often observed at the peripheries of vent communities (Gebruk et al., 2000b). Hence, we assume that *Alvinocaris* sp. aff. *stactophila* was present among the shrimps in the mussel beds.

5.3. Bathymodiolus azoricus area calculations

Bathymodiolus coverage was estimated at each site by delineating each individual patch of bivalves into a GIS. The smallest areas of mussel coverage were measured at Cage site and Atos 10, with respectively 12.3 m^2 and 13.2 m^2, while the largest coverage areas occurred at Woody with 17 m^2 and at White Flames with 29.1 m^2. From those data, it is not clear whether the extent of the mussel coverage is correlated to the size of the sites (Table 2). Data from Atos 10, Woody and White Flames suggest that larger sites host a larger mussel population. However, data from Cage Site, the second largest of the studied sites, suggest otherwise. The comparatively low mussel coverage of Cage Site could be related to a different fluid chemistry than at Atos 10, Woody and White Flames. Although we do not have fluid chemistry data to support this hypothesis, we know that Cage Site and Marker 4 are located in a different cluster than the other sites (Fig. 1c). Barreyre et al. (2012) proposed that the spatial distribution of active sites at Lucky Strike may reflect "the geometry of the underlying plumbing system". Such an interpretation implies that the larger the distance between outflows, the greater the differences in fluid composition. This would support the hypothesis that the fluid chemistry may be different between the two clusters described in this study.

Likewise, we could not correlate mussel coverage and fluid flow intensity from our data. Although the imagery data gave a reasonable view of the distribution (Figs. 3–5 and 7) and amount (Table 2) of focused outflows at each site, it did not make it possible to assess the size of focused outflows reliably enough to compare fluid flow intensity between sites. Moreover, it appears that the number of discrete outflows alone may not be representative of the strength of fluid flow. Indeed, Woody, the second largest site in terms of mussel cover, has fewer discrete outflows than Atos 10, Cage Site, and White Flames.

Similarly, zones of diffuse fluids could not be defined and, therefore, a comparison of diffuse fluid occurrence between sites

could not be done. Indeed, the main indicators for diffuse fluid flow that can be observed on imagery data of hydrothermal vents are bacterial mats and anhydrite precipitates (Barreyre et al., 2012). However, bacterial mats were rarely observed at the Menez Gwen sites, and diffuse fluid-related precipitates could not, in most cases, be unequivocally distinguished from precipitates related to focused fluid flow.

It is difficult to compare our estimates of mussel coverage to other hydrothermal vents because calculations of mussel coverage area are rarely available. An exception is the Logatchev hydrothermal vent field where *Bathymodiolus puteoserpentis* forms a large and continuous mussel bed of at least 100 m^2 at the base of the Irina-2 sulfide mound (Gebruk et al., 2000a). However, the extension of the Irina-2 mussel bed at Logatchev is controlled by the special underlying local geology. Logatchev is an ultramafic system characterized by serpentinization processes. The Irina-2 mussel bed is situated on silicified crusts that are underlain by sulfide fragments and chalcopyrite sand grading into serpentinite mud (Petersen et al., 2009). This incoherent underlying material provides many conduits for rising hydrothermal fluids that mix in the subsurface with entrained bottom water and exit the silicified crusts via many diffuse outlets spread over a large area (Petersen et al., 2009). Conversely, Menez Gwen is a basaltic-hosted system in which subsurface fluid conduits are controlled by basaltic rock. Fluid discharge is much more focused and colonization of mussels is predominantly confined to rock surfaces next to this focused discharge.

Other values of *Bathymodiolus* bottom coverage are available for two 50.3-m^2 and 40-m^2 large mosaics of diffuse flow areas at vents in the Eastern Lau Spreading Center of the western Pacific (Podowski et al., 2009). Here, the given values of site areas correspond to the mosaic areas. The dimensions of the actual sites of diffuse flow are not known and are potentially larger, making it impossible to assess the percentages of cover. However, the mussel *Bathymodiolus brevior* alone covered bottom areas of 3.8 m^2 and 0.72 m^2 and it is believed to be in competition with the provannid snail *Ifremeria nautilei* over additional areas of 3.8 m^2 and 0.6 m^2 (Podowski et al., 2009). The relation of the values to the size of the study areas is similar to this relation at Menez Gwen.

5.4. B. azoricus biomass estimations

Based on our measured values of mussel coverage (Table 2), population assessments (Table 3) ranged from about 4900 to 8600 ind at Cage Site (the least populated site) and from 11,600 to more than 20,000 ind at White Flames (the most populated site). The smallest biomass values were calculated for Cage Site with between 9 and 65 kg wet wt, and the largest for White Flames with between 21 and more than 154 kg wet wt. These are the first estimates of total mussel biomass on entire hydrothermal vent sites, while all other published values use the standardized unit kg m^{-2}. In the absence of data about the size of the mussel beds at the other sites, the total biomasses cannot be compared.

Published data for mussel biomass at hydrothermal vents or hydrocarbon seeps are rare and most of them range from 2.2 to 10 kg m^{-2} (Table 4), while a single peak value of 43.4 kg m^{-2} has been reported from the Oasis vent field on the Southern East Pacific Rise (Sarrazin et al., 2006). Compared to these values, a mussel biomass of 0.71 to 5.3 kg m^{-2} at Menez Gwen appears low. Nevertheless, this range is in accordance with the biomass estimation for *B. azoricus* at Lucky Strike (3.5 kg m^{-2}) (Van Dover et al., 1996).

5.5. Methane and sulfide consumption by B. azoricus

Hydrothermal fluids at Menez Gwen are relatively enriched in dissolved gas (Charlou et al., 2000), some of which are partly consumed by *B. azoricus*. Indeed, *Bathymodiolus* species are characterized by a great abundance of symbionts in their gills and by depleted isotopic carbon signatures in their tissues, which indicates that *Bathymodiolus* species from hydrothermal vents and hydrocarbon seeps primarily rely on the chemosynthetic production of the symbionts (Le Pennec et al., 1990; Raulfs et al., 2004). *Bathymodiolus azoricus* harbor sulfur oxidizing and methane oxidizing symbionts in their gills, which provide the host with metabolites from chemosynthetic oxidation of both volatiles present in the Menez Gwen hydrothermal fluids (Duperron et al., 2006; Fiala-Médioni et al., 2002). However, *Bathymodiolus* can filter feed (Page et al., 1990; Riou et al., 2010), and although the relative contribution of filter feeding to the nutrition of hosts has never been evaluated experimentally, recent modeling results suggest that particulate organic matter (POM) contributes to 48% to the nutrition of *B. azoricus* at Menez Gwen. Consequently, 52% of their nutrition is derived by symbiotic chemosynthesis that is fueled by oxidation of sulfide and methane (Martins et al., 2008).

Based on our assumptions of chemical uptake rates by the mussels (Table 1) and the calculated population size (Table 3), we provided minimum and maximum estimates of the annual methane and sulfide consumption at each study site (Table 3). The minimum estimates were obtained by combining the low limit (40 mm) of shell lengths range given by Comtet and Desbruyères (1998) with the lowest published estimate of mussel density at Menez Gwen (400 ind m^{-2}) (Colaço et al., 1998). The maximum estimate was using the corresponding upper limits of shell length and mussel density (SL=80 mm, density=700 ind m^{-2}) (Colaço et al., 1998; Comtet and Desbruyères, 1998). Therefore, the minimum and maximum scenarios provide very broad ranges for the estimated annual consumption of methane and sulfide by *B. azoricus*. Indeed, according to these calculations, the annual methane and sulfide consumption of population of *B. azoricus* at the study sites was estimated to range between 62 and 1760 mol CH_4 and between 382 and 11,060 mol H_2S. Such ranges reflect the uncertainties of our assumptions. Future measurements of mussel size distribution, density and chemical uptake rates should help constraining these estimates further.

The estimation method for uptake rates of methane and sulfide by *B. azoricus* (Martins et al., 2008) does not take into account the recent discovery that hydrogen also fuels endosymbiosis in *Bathymodiolus* mussels on the MAR (Petersen et al.,

Table 4
Published biomass estimates of mussels at hydrothermal vent and cold seep systems.

Site	Biomass (wet weight)	Reference
Galapagos	10.1 kg m^{-2}	Hessler and Smithey (1983)
Galapagos Ridge	2.2 kg m^{-2}	Fustec et al. (1988)
EPR	44.5 kg m^{-2} (tubeworms/mussels)	Desbruyères and Laubier (1991)
Lucky Strike	3.5 kg m^{-2}	Van Dover et al. (1996)
Barbados Prism	5.4–9 kg m^{-2}	Olu et al. (1996)
Oasis vent, SEPR	43.4 kg m^{-2}	Sarrazin et al. (2006)
Menez Gwen	0.71–5.3 kg m^{-2}	Assessed from Martins et al. (2008)

2011). With an average value of 38 μmol kg^{-1} the hydrogen concentration of Menez Gwen fluids is considered to be low in comparison to other vent systems (Charlou et al., 2000). This could imply that hydrogen consumption by mussels at Menez Gwen is low in comparison to sulfide and methane consumption. Nevertheless, these are the first estimates of total consumption of methane and sulfide by *B. azoricus* over entire sites of active venting. Although we cannot provide a comparison with similar estimates from other hydrothermal vent systems, these values could serve for future comparisons with other sites.

5.6. Methane and sulfide effluxes

In order to put these estimates of chemical consumption by the mussel population into a broader perspective, we need to look at the chemical fluxes that are potentially released via venting. Focused fluids are generally expelled vertically and vigorously into the water column (Sarrazin et al., 2009), and it is clear that a large fraction of these fluids is unavailable to the fauna at the seafloor. However, the aim of this section is to assess whether the faunal consumption is significant in comparison to the natural chemical release; in other words, in the absence of mussels, would the chemical release to the hydrosphere be significantly larger?

Previous estimates of chemical fluxes at Menez Gwen do not exist but can, within orders of magnitude, be estimated from published fluid data (Charlou et al., 2000) and estimates of fluid flow rates. Hydrothermal fluids at Menez Gwen are relatively enriched in dissolved gas. For instance, mean end-member methane and sulfide concentrations were estimated at 1.7 mmol CH_4/kg and 1.6 mmol H_2S/kg (Charlou et al., 2000). Considering a fluid density at Menez Gwen of 733 kg/m^3 (Charlou et al., 2000), the smallest discrete outflows (diameter = 0.5 cm, area = 0.2 cm^2) could yield down to 77 mol CH_4 yr^{-1} and 73 mol H_2S yr^{-1} (for a fluid velocity of 100 mm yr^{-1}), while the largest observed outflow (diameter = 12 cm, area = 113.1 cm^2) could yield up to 2.8×10^6 mol CH_4 yr^{-1} and 2.6×10^6 mol H_2S yr^{-1} (for a maximum fluid velocity of 6200 mm yr^{-1}). However, these values are based on extreme values of plume diameter that are not representative of an average-size discrete outflow at Menez Gwen; thus they are not appropriate to estimate the global release of methane and sulfide at the scale of the studied sites. Furthermore, the plume diameter could be estimated for a subset only of the total discrete sources (24 out of 92), hence we cannot reliably constrain the estimates of methane and sulfide release further. Nevertheless, if we consider that a diameter of 2 cm is representative of an average discrete outflow (cf. Section 3.5 for details), the total focused discharge in the area of study could sum up to 91,000 m^3 yr^{-1} (minimum estimate based on a fluid velocity of 100 mm yr^{-1}). This corresponds to total annual releases of methane and sulfide via discrete venting of 113×10^3 mol CH_4 yr^{-1} and 107×10^3 mol H_2S yr^{-1}. These values are based on low limit estimates of fluid velocity and of median plume size; in particular, they do not take into account the presence of an extremely large discrete outflow (cf. Section 3.5 for details). Hence, they likely underestimate significantly the actual chemical fluxes. Notwithstanding these caveats, our estimates suggest that methane and sulfide consumption by the mussel population represents a small fraction of fluxes potentially released from the system into the water column. Indeed, according to these estimations, the mussel consumption would represent up to 1.6% of the methane and 10.4% of the sulfide fluxes released via focused venting.

Areas of diffuse outflow were not easily identified from the imagery data and could not be quantified. Based on mosaics of Lucky Strike, Barreyre et al. (2012) suggest several types of diffuse flow-related features. Some of these, such as bacterial mats and patches of hydrothermal precipitates, occurred in the studied sites. However, bacterial mats were rarely observed at the Menez Gwen sites, and diffuse fluid-related precipitates could not, in most cases, be unequivocally distinguished from precipitates related to focused fluid flow. For these reasons, diffuse flow rates could not be quantified for the entire site. Nevertheless, available data allow us to estimate the order of magnitude of diffusive chemical fluxes. According to Sarrazin et al. (2009), existing velocity measurements of diffuse fluids in hydrothermal systems range from 1.1 to 150 mm s^{-1} in diffuse sources. Therefore, using the low range limit value of 1 mm s^{-1}, diffuse chemical fluxes could be in the order of at least 54×10^3 mol CH_4 m^{-2} yr^{-1} and 50×10^3 mol H_2S m^{-2} yr^{-1}. Based on these values of diffuse chemical fluxes, diffuse venting over a 1 m^2 area could meet respectively 30 and 4.5 times the total mussel consumption of methane and sulfide in the entire studied area. However, methane and sulfide concentrations in diffuse fluids are expected to be lower than in focused fluids due to mixing with sea water; therefore, diffuse chemical fluxes are probably lower than our estimations (for a given fluid velocity).

A few values of methane fluxes within hydrothermal plumes have been published for other vent fields with similarly high end-member methane concentrations. All are at least 3 orders of magnitude higher than our estimates of methane fluxes at Menez Gwen. For instance, methane fluxes of about 132×10^6 mol yr^{-1} were estimated in the plume 200 m above the Endeavor vent field on the Juan de Fuca Ridge (Rosenberg et al., 1988). Similarly, published estimates of helium isotope ^{3}He flux and of the $CH_4/^3$He ratio at the Rainbow hydrothermal vent on the MAR suggest a methane flux of 50.8×10^6 mol yr^{-1} for a plume that includes all hot fluid flow emanating from a 100×200 m^2-large area (Jean-Baptiste et al., 2004). Furthermore, for the same plume, German et al. (2010) inferred a methane flux of 31.6×10^6 mol yr^{-1} by establishing a linear relationship between methane concentrations and "plume-particle" fluxes from optical backscatter anomalies. Finally, Keir et al. (2008) calculated methane fluxes at the solitary "Drachenschlund" black smoker vent in the "Nibelungen" hydrothermal vent field on the Southern MAR ranging from 1.8×10^6 mol yr^{-1} at the vent itself to 15.8×10^6 mol yr^{-1} in the horizontal plume. All these systems emit hot fluids with high methane concentrations (Lilley et al., 1993; Charlou et al., 2002; Melchert et al., 2008) similar to those measured at Menez Gwen (Charlou et al., 2000), even though their geological settings are different.

These comparisons could imply that the Menez Gwen sites are minor in terms of chemical release. However, our estimates of fluid flow and chemical fluxes were purposely low and aimed at assessing the relative importance of chemical consumption by the mussel. Indeed, according to available fluid velocity measurements (Sarrazin et al., 2009), actual fluid flow rates and chemical fluxes at Menez Gwen could be higher than our estimates by more than an order of magnitude.

6. Conclusions

The zones of active venting have very limited extents and are mainly concentrated on the flanks of a mini-volcano close to the center of the Menez Gwen volcano. The faunal distribution at the studied sites is very similar to that at the Eiffel Tower structure in the neighboring Lucky Strike vent field (Cuvelier et al., 2009). The fauna at the studied Menez Gwen sites is dense and largely dominated by *Bathymodiolus azoricus*. Patches of mussels are mostly distributed on hard substrata on the pathway of the hot fluid but preferentially away from the chimney flanks. Populations of more mobile taxa such as shrimps and gastropods are clearly denser in the vicinity of points of fluid emission. Nevertheless, this behavior was not observed at every point of venting activity. Good examples are

the large chimneys at the top of White Flames site, where the venting fluid appears as if boiling.

Despite the small extent of the sites of active venting, the mussel population amounts to thousands of individuals and estimates of the minimum total biomass over the sites of study total hundreds of kilograms. The estimates of total annual consumption of methane and sulfide by *B. azoricus* can be significant, and respectively up to 1760 mol CH_4 yr^{-1} and 11,060 mol H_2S yr^{-1}. The chemical consumption seems nevertheless low in comparison to estimates of vent-scale hydrothermal methane and sulfide effluxes. However, this work considered the consumption by mussels only, and the total consumption by all symbiotic fauna may be more substantial. Nevertheless, *B. azoricus* was the dominant species at these sites and, therefore, the total consumption by the fauna is likely to be in the same order of magnitude.

Geo-referenced photomosaics and geographic information systems constitute efficient tools to observe the faunal distribution and are amongst the most accurate tools available for areal calculations in such remote environments. Estimating the total biomass of *B. azoricus* at every site was only possible with accurate estimates of the extent of the mussel patches. The photomosaics presented in this work are also aimed at giving a snapshot of the situation at Menez Gwen in 2010 and can serve for future works as basemaps for planning or site recognition purposes. They also are a good basis to observe the temporal evolution of the venting and faunal activity.

Acknowledgments

We would like to thank Nicole Dubilier, chief scientist of M82/3 cruise, the captain and crew of RV Meteor, and the ROV Quest team. Also thanks to Elizabeth L. Podowski, Charles R. Fisher and Stephanie Lessard-Pilon. Finally, we thank the associate editor Andy Gooday and the three reviewers, who put a lot of efforts into improving this study.

This work was supported by the European Commission under the EU Framework 7 funded Marie Curie Initial Training Network (ITN) SENSEnet (contract n°237868), and funded through DFG Research Center/Excellence Cluster "The Ocean in the Earth System".

Appendix A. Supporting information

Supplementary data associated with this article can be found in the online version at http://dx.doi.org/10.1016/j.dsr.2013.01.008.

References

Abramoff, M.D., Magalhães, P.J., Ram, S.J., 2004. Image processing with image. J. Biophotonics Int. 11, 36–42.

Barreyre, T., Escartín, J., Garcia, R., Cannat, M., Mittelstaedt, E., Prados, R., 2012. Structure, temporal evolution, and heat flux estimates from the Lucky Strike deep-sea hydrothermal field derived from seafloor image mosaics. Geochem. Geophys. Geosyst. 13, 29.

Bell, K.L.C., Nomikou, P., Carey, S.N., Stathopoulou, E., Polymenakou, P., Godelitsas, A., Roman, C., Parks, M., 2012. "Continued Exploration of the Santorini Volcanic Field and Cretan Basin, Aegean Sea" in New Frontiers in Ocean Exploration: The E/V *Nautilus* and NOAA Ship *Okeanos Explorer* 2011 Field Season by Bell, K.L.C., K. Elliott, C. Martinez, S.A. Fuller (Eds.), 2012. Oceanography, vol. 25, pp. 30–31.

Caress, D.W., Chayes, D.N., 2001. Improved Management of Large Swath Mapping Datasets in MB-System Version 5. AGU Fall Meeting Abstracts.

Charlou, J.L., Donval, J.P., Douville, E., Jean-Baptiste, P., Radford-Knoery, J., Fouquet, Y., Dapoigny, A., Stievenard, M., 2000. Compared geochemical signatures and the evolution of Menez Gwen (37°50′N) and Lucky Strike (37°17′N) hydrothermal fluids, south of the Azores Triple Junction on the Mid-Atlantic Ridge. Chem. Geol. 171, 49–75.

Charlou, J.L., Donval, J.P., Fouquet, Y., Jean-Baptiste, P., Holm, N., 2002. Geochemistry of high H2 and CH4 vent fluids issuing from ultramafic rocks at the Rainbow hydrothermal field (36°14′N, MAR). Chem. Geol. 191, 345–359.

Colaço, A., Desbruyères, D., Comtet, T., Alayse, A.M., 1998. Ecology of the Menez Gwen hydrothermal vent field (Mid-Atlantic Ridge/Azores Triple Junction). Cah. Biol. Mar. 39, 237–240.

Comtet, T., Desbruyères, D., 1998. Population structure and recruitment in mytilid bivalves from the Lucky Strike and Menez Gwen hydrothermal vent fields (37°17′N and 37°50′N on the Mid-Atlantic Ridge). Mar. Ecol. Prog. Ser. 163, 165–177.

Copley, J., Tyler, P.A., Murton, B.J., Van Dover, C.L., 1997. Spatial and interannual variation in the faunal distribution at Broken Spur vent field (29°N, Mid-Atlantic Ridge). Mar. Biol. 129, 723–733.

Cuvelier, D., Sarrazin, J., Colaço, A., Copley, J., Desbruyères, D., Glover, A.G., Tyler, P., Serrão-Santos, R., 2009. Distribution and spatial variation of hydrothermal faunal assemblages at Lucky Strike (Mid-Atlantic Ridge) revealed by high-resolution video image analysis. Deep-Sea Res. Part I 56, 2026–2040.

Delaney, J.R., Robigou, V., McDuff, R.E., Tivey, M.K., 1992. Geology of a vigorous hydrothermal system on the Endeavor segment, Juan de Fuca Ridge. J. Geophys. Res. 97, 663–682.

Desbruyères, D., Biscoito, M., Caprais, J.C., Colaço, A., Comtet, T., Crassous, P., Fouquet, Y., Khripounoff, A., Le Bris, N., Olu, K., Riso, R., Sarradin, P.M., Segonzac, M., Vangriesheim, A., 2001. Variations in deep-sea hydrothermal vent communities on the Mid-Atlantic Ridge near the Azores plateau. Deep-Sea Res. Part I 48, 1325–1346.

Desbruyères, D., Laubier, L., 1991. Systematics, phylogeny, ecology and distribution of the Alvinellidae (Polychaeta) from deep-sea hydrothermal vents. Ophelia 5, 31–45.

Dixon, D.R., Dando, P.R., Santos, R.S., Gwynn, J.P., 2001. VENTOX, C., 2001. Retrievable cages open up new era in deep-sea vent research. InterRidge News 10 (2), 21–23.

Duperron, S., Bergin, C., Zielinski, F., Blazejak, A., Pernthaler, A., McKiness, Z.P., DeChaine, E., Cavanaugh, C.M., Dubilier, N., 2006. A dual symbiosis shared by two mussel species, *Bathymodiolus azoricus* and *Bathymodiolus puteoserpentis* (Bivalvia: Mytilidae), from hydrothermal vents along the northern Mid-Atlantic Ridge. Environ. Microbiol. 8, 1441–1447.

Durand, S., Le Bel, M., Juniper, S.K., Legendre, P., 2002. The use of video surveys, a Geographic Information System and sonar backscatter data to study faunal community dynamics at Juan de Fuca Ridge hydrothermal vents. Cah. Biol. Mar. 43, 235–240.

Escartín, J., García, R., Delaunoy, O., Ferrer, J., Gracias, N., Elibol, A., Cufi, X., Neumann, L., Fornari, D.J., Humphris, S.E., Renard, J., 2008. Globally aligned photomosaic of the Lucky Strike hydrothermal vent field (Mid-Atlantic Ridge, 37°18.5′N): Release of georeferenced data, mosaic construction, and viewing software. Geochem. Geophys. Geosyst. 9, 17.

Fiala-Médioni, A., McKiness, Z.P., Dando, P., Boulegue, J., Mariotti, A., Alayse-Danet, A.M., Robinson, J.J., Cavanaugh, C.M., 2002. Ultrastructural, biochemical, and immunological characterization of two populations of the mytilid mussel *Bathymodiolus azoricus* from the Mid-Atlantic Ridge: evidence for a dual symbiosis. Mar. Biol. 141, 1035–1043.

Fouquet, Y., Charlou, J.L., Costa, I., Donval, J.P., Radford-Knoery, J., Pellé, H., Ondréas, H., Lourenco, N., Segonzac, M., Tivey, M.K., 1994. Detailed Study of the Lucky Strike Hydrothermal Site and Discovery of a New Hydrothermal Site: Menez Gwen; Preliminary Results of the DIVA1 Cruise (5–29 May, 1994). InterRidge News 3 (2), 14–17.

Fouquet, Y., Ondréas, H., Charlou, J.L., Donval, J.P., Radford-Knoery, J., Costa, I., Lourenco, N., Tivey, M.K., 1995. Atlantic lava lakes and hot vents. Nature 377, 201.

Fouquet, Y., Schultz, A., Fouquet, Y., Herrington, R., Nesbitt, R.W., 1997. Where are the large hydrothermal sulphide deposits in the oceans? Philos. Trans.: Math. Phys. Eng. Sci. 355, 427–441.

Fustec, A., Desbruyères, D., Laubier, L., 1988. Estimation de la biomasse des peuplements associés aux sources hydrothermales profondes de la dorsale du Pacifique oriental à 13°N. Oceanol. Acta 8, 15–21.

Galkin, S.V., Goroslavskaya, E.I., 2010. Bottom fauna associated with *Bathymodiolus azoricus* (Mytilidae) mussel beds in the hydrothermal fields of the Mid-Atlantic Ridge. Oceanology 50, 51–60.

Gebruk, A.V., Chevaldonné, P., Shank, T., Lutz, R.A., Vrijenhoek, R.C., 2000a. Deep-sea hydrothermal vent communities of the Logatchev area (14°45′N, Mid-Atlantic Ridge): diverse biotopes and high biomass. J. Mar. Biol. Assoc. UK 80, 383–393.

Gebruk, A.V., Southward, E.C., Kennedy, H., Southward, A.J., 2000b. Food sources, behaviour, and distribution of hydrothermal vent shrimps at the Mid-Atlantic Ridge. J. Mar. Biol. Assoc. UK 80, 485–499.

German, C.R., Thurnherr, A.M., Knoery, J., Charlou, J.L., Jean-Baptiste, P., Edmonds, H.N., 2010. Heat, volume and chemical fluxes from submarine venting: A synthesis of results from the Rainbow hydrothermal field, 36°N MAR. Deep-Sea Res. Part I 57, 518–527.

Grehan, A.J., Juniper, S.K., 1996. Clam distribution and subsurface hydrothermal processes at Chowder Hill (Middle Valley), Juan de Fuca Ridge. Mar. Ecol. Prog. Ser. 130, 105–115.

Hessler, R.R., Smithey, W.M., 1983. Hydrothermal processes at seafloor spreading centers, NATO Conference Series. IV, Marine Sciences. Plenum Press, New York, N.Y.

Jean-Baptiste, P., Fourré, E., Charlou, J.L., German, C.R., Radford-Knoery, J., 2004. Helium isotopes at the Rainbow hydrothermal site (Mid-Atlantic Ridge, 36°14′N). Earth Planet. Sc. Lett. 221, 325–335.

Jerosch, K., Lüdtke, A., Schlüter, M., Ioannidis, G.T., 2007. Automatic content-based analysis of georeferenced image data: detection of Beggiatoa mats in seafloor video mosaics from the Håkon Mosby Mud Volcano. Comput. Geosci. 33, 202–218.

Jerosch, K., Schlüter, M., Pesch, R., 2006. Spatial analysis of marine categorical information using indicator kriging applied to georeferenced video mosaics of the deep-sea Håkon Mosby Mud Volcano. Ecol. Inform. 1, 391–406.

Judd, A.G., 2003. The global importance and context of methane escape from the seabed. Geo-Mar. Lett. 23, 147–154.
Juniper, S.K., Sarrazin, J., Grehan, A., 1998. Remote sensing of organism density and biomass at hydrothermal vents. Cah. Biol. Mar. 39, 245–247.
Keir, R.S., Schmale, O., Walter, M., Sültenfuß, J., Seifert, R., Rhein, M., 2008. Flux and dispersion of gases from the "Drachenschlund" hydrothermal vent at 8°18' S, 13°30' W on the Mid-Atlantic Ridge. Earth Planet. Sc. Lett. 270, 338–348.
Le Pennec, M., Donval, A., Herry, A., 1990. Nutritional strategies of the hydrothermal ecosystem bivalves. Prog. Oceanogr. 24, 71–80.
Lessard-Pilon, S.A., Podowski, E.L., Cordes, E.E., Fisher, C.R., 2010a. Megafauna community composition associated with *Lophelia pertusa* colonies in the Gulf of Mexico. Deep-Sea Res. Part II 57, 1882–1890.
Lessard-Pilon, S.A., Porter, M.D., Cordes, E.E., MacDonald, I.R., Fisher, C.R., 2010b. Community composition and temporal change at deep Gulf of Mexico cold seeps. Deep-Sea Res. Part II 57, 1891–1903.
Lilley, M.D., Butterfield, D.A., Olson, E.J., Lupton, J.E., Macko, S.A., McDuff, R.E., 1993. Anomalous CH4 and NH4+ concentrations at an unsedimented mid-ocean-ridge hydrothermal system. Nature 364, 45–47.
Lutz, R.A., Kennish, M.J., 1993. Ecology of deep-sea hydrothermal vent communities: a review. Rev. Geophys. 31, 211–242.
Martins, I., Colaço, A., Dando, P.R., Martins, I., Desbruyères, D., Sarradin, P.M., Marques, J.C., Serrão-Santos, R., 2008. Size-dependent variations on the nutritional pathway of *Bathymodiolus azoricus* demonstrated by a C-flux model. Ecol. Model. 217, 59–71.
Melchert, B., Devey, C.W., German, C.R., Lackschewitz, K.S., Seifert, R., Walter, M., Mertens, C., Yoerger, D.R., Baker, E.T., Paulick, H., Nakamura, K., 2008. First evidence for high-temperature off-axis venting of deep crustal/mantle heat: The Nibelungen hydrothermal field, southern Mid-Atlantic Ridge. Earth Planet. Sc. Lett. 275, 61–69.
Olu, K., Sibuet, M., Harmegnies, F., Foucher, J.P., Fiala-Médioni, A., 1996. Spatial distribution of diverse cold seep communities living on various diapiric structures of the southern Barbados prism. Prog. Oceanogr. 38, 347–376.
Olu-Le Roy, K., Caprais, J.C., Fifis, A., Fabri, M.C., Galéron, J., Budzinsky, H., Le Ménach, K., Khripounoff, A., Ondréas, H., Sibuet, M., 2007. Cold-seep assemblages on a giant pockmark off West Africa: spatial patterns and environmental control. Mar. Ecol. 28, 115–130.
Ondréas, H., Fouquet, Y., Voisset, M., Radford-Knoery, J., 1997. Detailed study of three contiguous segments of the Mid-Atlantic Ridge, south of the Azores (37 N to 38 30′ N), using acoustic imaging coupled with submersible observations. Mar. Geophys. Res. 19, 231–255.
Page, H.M., Fisher, C.R., Childress, J.J., 1990. Role of filter-feeding in the nutritional biology of a deep-sea mussel with methanotrophic symbionts. Mar. Biol. 104, 251–257.
Parson, L., Grācia, E., Coller, D., German, C., Needham, D., 2000. Second-order segmentation; the relationship between volcanism and tectonism at the MAR, 38°N–35° 40′N. Earth Planet. Sci. Lett. 178, 231–251.
Petersen, J.M., Zielinski, F.U., Pape, T., Seifert, R., Moraru, C., Amann, R., Hourdez, S., Girguis, P.R., Wankel, S.D., Barbe, V., Pelletier, E., Fink, D., Borowski, C., Bach, W., Dubilier, N., 2011. Hydrogen is an energy source for hydrothermal vent symbioses. Nature 476, 176–180.
Petersen, S., Kuhn, K., Kuhn, T., Augustin, N., Hékinian, R., Franz, L., Borowski, C., 2009. The geological setting of the ultramafic-hosted Logatchev hydrothermal field (14°45′N, Mid-Atlantic Ridge) and its influence on massive sulfide formation. Lithos 112, 40–56.
Pizarro, O., Singh, H., 2003. Toward large-area mosaicing for underwater scientific applications. IEEE J. Oceanic Eng. 28, 651–672.
Podowski, E.L., Moore, T.S., Zelnio, K.A., Luther III, G.W., Fisher, C.R., 2009. Distribution of diffuse flow megafauna in two sites on the Eastern Lau Spreading Center, Tonga. Deep-Sea Res. Part I 56, 2041–2056.
Ramirez Llodra, E., Shank, T.M., German, C.R., 2007. Biodiversity and biogeography of hydrothermal vent species: thirty years of discovery and investigations. Oceanography 20, 30–41.
Ramirez Llodra, E., Tyler, P.A., Copley, J., 2000. Reproductive biology of three caridean shrimp, *Rimicaris exoculata, Chorocaris chacei* and *Mirocaris fortunata* (Caridea: Decapoda), from hydrothermal vents. J. Mar. Biol. Assoc. UK 80, 473–484.
Raulfs, E.C., Macko, S.A., Van Dover, C.L., 2004. Tissue and symbiont condition of mussels (*Bathymodiolus thermophilus*) exposed to varying levels of hydrothermal activity. J. Mar. Biol. Assoc. UK 84, 229–234.
Riou, V., Duperron, S., Halary, S., Dehairs, F., Bouillon, S., Martins, I., Colaço, A., Serrão-Santos, R., 2010. Variation in physiological indicators in Bathymodiolus azoricus (Bivalvia: Mytilidae) at the Menez Gwen Mid-Atlantic Ridge deep-sea hydrothermal vent site within a year. Mar. Environ. Res. 70, 264–271.
Sarradin, P.M., Caprais, J.C., Riso, R., Comtet, T., Aminot, A., 1998. Brief account of the chemical environment at hydrothermal vent mussel beds on the MAR. Cah. Biol. Mar. 39, 253–254.
Sarradin, P.M., Caprais, J.C., Riso, R., Kerouel, R., Aminot, A., 1999. Chemical environment of the hydrothermal mussel communities in the Lucky Strike and Menez Gwen vent fields, Mid Atlantic Ridge. Cah. Biol. Mar. 40, 93–104.
Sarradin, P.M., Desbruyères, D., Dixon, D.R., Almeida, A., Briand, P., Caprais, J.C., Colaço, A., Company, R., Cosson, R., Cueff, V., Dando, P., Etoubleau, J., Fabri, M.C., Fiala-Medioni, A., Gaill, F., Godfroy, A., Gwynn, J.P., Hourdez, S., Jollivet, D., Khripounoff, A., Lallier, F.H., Laulier, M., Le Bris, N., Martins, I., Mestre, N., Pruski, A., Rodier, P., Serrão-Santos, R., Shillito, B., Zal, F., Zbinden, M., 2001. ATOS cruise R/V L'Atalante, ROV Victor, June 22nd–July 21st 2001. InterRidge News 10 (2), 18–20.
Sarrazin, J., Juniper, S.K., 1998. The use of video imagery to gather biological information at deep-sea hydrothermal vents. Cah. Biol. Mar. 39, 255–258.
Sarrazin, J., Robigou, V., Juniper, S.K., Delaney, J.R., 1997. Biological and geological dynamics over four years on a high-temperature sulfide structure at the Juan de Fuca Ridge hydrothermal observatory. Mar. Ecol. Prog. Ser. 153, 5–24.
Sarrazin, J., Rodier, P., Tivey, M.K., Singh, H., Schultz, A., Sarradin, P.M., 2009. A dual sensor device to estimate fluid flow velocity at diffuse hydrothermal vents. Deep-Sea Res. Part I 56, 2065–2074.
Sarrazin, J., Walter, C., Sarradin, P.M., Brind'Amour, A., Desbruyères, D., Briand, P., Fabri, M.C., Van Gaever, S., Vanreusel, A., Bachraty, C., Thiebaut, E., 2006. Community structure and temperature dynamics within a mussel assemblage on the Southern East Pacific Rise. Cah. Biol. Mar. 47, 483–490.
Shank, T.M., Martin, J.W., 2003. A new caridean shrimp of the family Alvinocarididae from thermal vents at Menez Gwen on the Mid-Atlantic Ridge. Proc. Biol. Soc. Wash. 116, 158–167.
Van Dover, C.L., 2000. The Ecology of Deep-Sea Hydrothermal Vents. Princeton Univ. Press, Princeton, N.J..
Van Dover, C.L., Desbruyères, D., Segonzac, M., Comtet, T., Saldanha, L., Fiala-Médioni, A., Langmuir, C., 1996. Biology of the Lucky Strike hydrothermal field. Deep-Sea Res. Part I 43, 1509–1529.
Von Cosel, R., Comtet, T., Krylova, E.M., 1999. *Bathymodiolus* (Bivalvia: Mytilidae) from hydrothermal vents on the Azores Triple Junction and the Logatchev hydrothermal field, Mid-Atlantic Ridge. Veliger 42, 218–248.